Dr. Nina Kirchner, Editor

Geoscientific Model Development

Subject: Revision submission

Dear Dr. Kirchner,

We thank you for handling our manuscript " MEMLS3&a: Microwave Emission Model of Layered Snowpacks adapted to include backscattering". Please find below our detailed replies to the comments by the Referees. We refer, where appropriate, to the marked-up manuscript.

We would like to express our sincere thanks to editors and reviewers for the detailed comments, which improved clarity and eliminated many larger and smaller errors.

Best regards,

Martin Proksch

on behalf of all authors

Answers to Referees

Below we address each point raised be the Referees in detail with our replies in blue and the *corrected/new text highlighted in green both in the replies below and in the revised manuscript.*

Anonymous Referee #1

General Comments: The topic of this article is a sophisticated model for simulating microwave emission and scattering of snow, which very well balances theoretical issues and practical handling. Such simulation models are essential when developing remote sensing technologies for continuous retrieval of snow properties over larger regions. Although the article is directly related to snow covers on land surfaces, it is useful also for snow on sea ice and for snow/firn of the ice sheets. The paper is very well written and structured and should definitely be published. I have only a few minor comments and questions.

We thank the reviewer for the constructive review and comments, which helped to improve the manuscript.

Specific comments

Page 2611, line 4: assumption of Lambertian reflectance: The intensity of surface scattering from ice and snow may reveal a dependence on the observer's zenith angle.Is the assumption of Lambertian reflectance (i. e. the apparent brightness of a surface does not depend on the observation angle) realistic in all cases? If not, what does this mean for the model simulations? (The text on page 2612 lines 15-19 implies that the Lambertian behavior is a consequence of the dominance of volume scattering?) Please comment.

In the model we divide specular and diffuse reflectivity. The diffuse part is indeed assumed as a consequence of volume scattering. The specular part is assumed as a consequence of specular reflections at the snow-ground interface, at the layer interfaces and at the snow-air interface. The recurrence relation of eq. 14 accounts for all these processes and finally eq. 15 gives the reflectivity of the entire snowpack-ground system. In this respect, the model is not only Lambertian. Further, the simulated brightness temperatures depend on the incidence angle as shown in Fig. 9, 10, 13.

Page 2612, line 9: How is the constant S_0 determined?

Page 2612, line 11: $S_0 = 4 r_d$

Page 2613: Equation 9 is the "geometric optics" (GO) model (Ulaby p. 983). The Physical Optics or Kirchhoff formulation (Ulaby p. 925-926) includes both GO and the scalar approximation.

We changed the sentence to:

"This equation corresponds to the geometrical-optics solution for undulating surfaces…"

Section 2.2. For a reader not familiar with passive radiometry one should mention how two different values of T_{sky} can be obtained in real measurement scenarios? (Referring to section 4.1.3 – use of measurements acquired at different air temperatures?)

In a real measurement scenario T_{sky} could be obtained as outlined in section 4.1.3. from radiometer measurements. Section 2.2 is only meant to derive the reflectivity r from brightness temperatures Tb1,Tb2 which were simulated for two arbitrary sky temperatures Tsky1, Tsky2, i.e. Section 2.2 does not require any measured T_{sky} values.

Page 2619, line15: Wasn't the snow temperature directly measured during the field measurements?

Due to time constrains, the snow temperature was not measured directly in the snow pit, but the taken from an automatic snow temperature measurements at the test site.

Page 2620, line 1: referring to the selection of the value of the frozen ground permittivity in line with Rautiainen et al. (2012) – the title of the Rautiainen-article suggests that the permittivity is valid at L-band, whereas here simulations are carried out at much higher frequencies?

Correct, the permittivities of Rautiainen were derived from L-band measurements. However, the frequency dependence of the frozen soil permittivity is not well known and therefore we used the Rautiainen et al., 2012 value as best guess.

Page 2621, Fig. 7 and Fig. 8: the latter repeats the results for CT-input already shown in Fig. 7? I would suggest to remove the CT-result from Fig. 7 and to mention that Fig. 8 specifically shows the "best" result.

A crucial part to model microwave emission/ backscatter is the derivation of the necessary input parameters. We wanted to show different methods how this can be done for MEMLS3&a, and also how those different methods compare then in terms of backscatter values. Therefore we think Fig.7 is useful and should contain the CT results, even if it is duplicated in Fig. 8.

Why did you select an incidence angle of 50° for this examples? Most satellite radar measurements are typically in the range between 25° and 40°.

50° is a standard value for radiometry. We wanted to compare the active and passive data at the same angle. For scatterometers, this corresponds to a common value, too (the fact that some radars are limited to smaller incidence angle is mainly due to technical limitations and not for physical reasons).

Page 2622, lines 3-5: The variations of the backscattered intensity due to fading can be estimated. Considering that the number of independent looks seems to be close to 40, the variations of the backscattering coefficient should be rather small. Can the authors definitely exclude variations of snow and ground properties? Looking at the results e. g. shown in Figs 9 and 10, this should be discussed more carefully.

We agree with the reviewer and added a comment about the influence of spatial variability:
The SnowScat observations at different incidence angles show a certain amount of scatter, which we attribute to the heterogeneity of the ground and snowcover at the test site.

Page 2624: I am somewhat uncertain whether I agree that the simulations are in "good" agreement with the SnowScat observations. Maybe "reasonable" is a better word, considering the results shown in Figs. 9 and 10, and also the problems with unknown input parameters (q, m, microstructure correlation function, frozen ground characteristics…)

We agree with the referee and changed the corresponding paragraphs.

Discussion: It would be useful to get an impression concerning the individual magnitudes of the surface/interface and the volume contribution (in particular for the case of dry snow).

We agree to the referee and included the following figure and text in the discussions on page 2625, line 12 ff.:
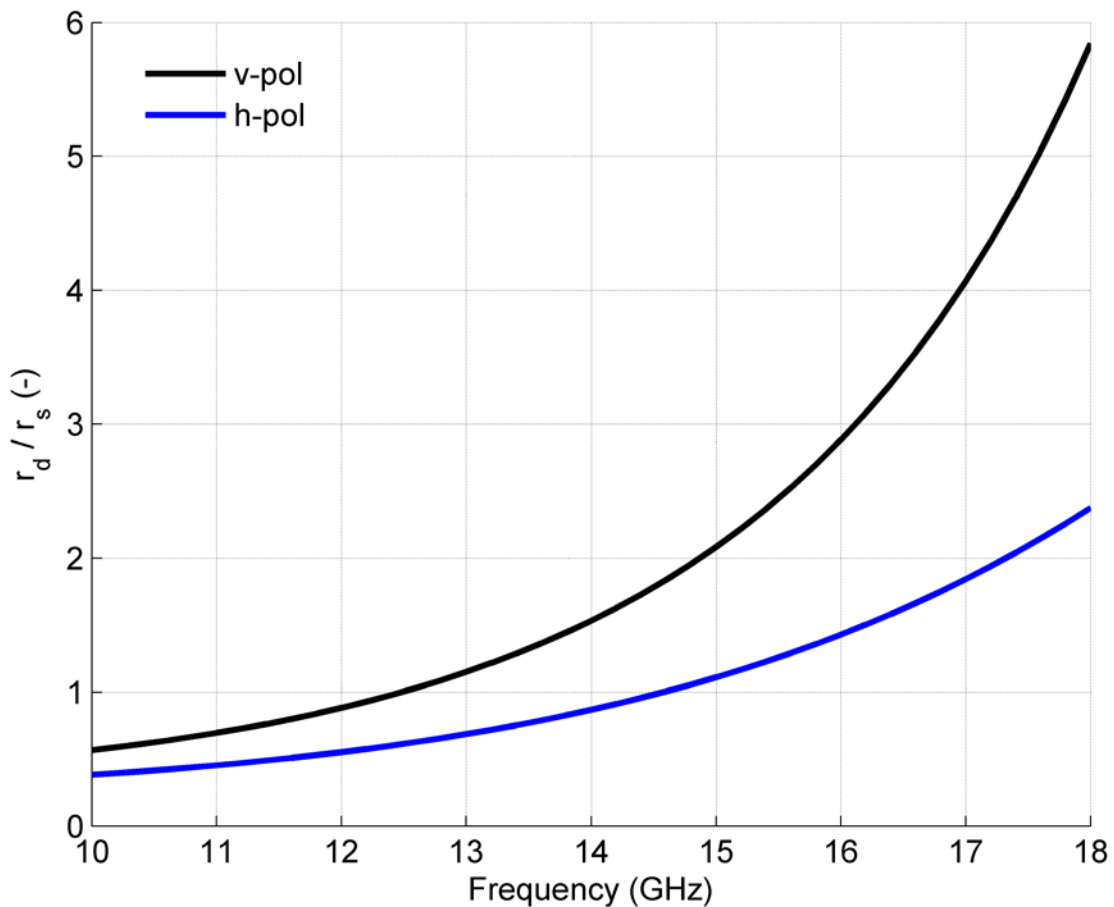
Fig: 16: Ratio of the simulated diffuse (r_d) and specular (r_s) reflectivity at 50° incidence angle per frequency, for the best fit parameters according to Fig 8.

The individual magnitudes of the specular and diffuse contributions are shown in Figure 16. Towards higher frequencies the diffuse component increases and outweighs the specular reflectivity from 12.5 GHz for v-pol and from 14.5 GHz for h-pol. Note that the magnitude of the specular component also depends on the undulation of the surface and therefore on the value of m. However, a pronounced impact of m is limited to small incidence angles (Fig. 13 and section 4.2.2) for reasonable values of m (m ~ 0.1).

Is the correlation length really a much better characteristic for quantifying the snow microstructure? The advantages of this approach are well described in the discussion (p. 2627) but I wonder whether situations may occur in which the knowledge of grain size distributions and grain cluster characteristics are better quantifiers of the snow microstructure, at least with regard to microwave scattering (theoretical scattering models based on the permittivity's correlation function also have limitations).

The correlation function is a classic descriptor of porous media (e.g. Torquato 2002, Löwe et al., 2011) such as snow. Models of grain size distributions would need at first a precise definition of grain size, which is often not congruent to what the microwave models use as microstructure length scale. In this respect, the correlation length/function provides an attractive starting point, as it is exactly the same parameter used in the model which is measured in the field. Correlation length can also be used to derive a second length scale (e.g. using the Teubner-Strey form) which then could

be used to account for effects like "clustering". A particular advantage of MEMLS3&a is that different types of correlation function could be included in the model by adapting the calculation of the scattering coefficient

Anonymous Referee #2
The author provides a clear detailed review of MEMLS3&a model. The extension of including the backscattering is documented with formulation, parameters setup and validation. In general, the paper is well written and the code provided is very useful to reproduce the results in the paper. However, there are still a few elements need to be elaborated and explained.

We thank the reviewer for the constructive review and comments, which helped to improve the manuscript.

1. Figure 13 needs more explanation. On page 2622, line21, the statement " The effect of m is limited to small incidence angles: : :" only explains the curves of m = 0.05 and m = 0.1. When m increase to 0.25, there is a dramatically change over 30-50 degree. However, compared to the SnowScat measurement, it seems when the MEMLS model match well with small m setting. Is that mean a smooth surface is sufficient for the match-up?

We agree that the formulation "The effect of m is limited to small incidence angles..." is not correct with respect to Figure 13 and deleted it. Page 2622, line21 now reads: *"A larger value of m represents a stronger undulated surface and increases the spectral component of the backscatter, in particular at small incidence angles. Fig. 13 shows this behavior, with increasing backscatter for increasing values of m and decreasing incidence angles. Given values smaller than 0.1, m has no effect at incidence angles larger than 25°. Further, cross polarization is in general not affected by m. Note that… "*

However, m is currently an empirical parameter, introduced to calculate specular backscatter from a slightly undulated slope, but remains a free parameter in the model so far. In principle, a "physical" value for m could be obtained from a detailed analysis of the snow surface (page 2625, line 3-10), and the values given in the literature (0.14) and used in this paper (0.1) are similar, but the relation between this "physical" or measured m and the m required by the model is not clear. As such, we can't really state that a smooth surface is sufficient for the match-up, but only that small values of m are sufficient.

2. The soil backscattering contribution can be significant in the lower frequency. It will be very helpful to include a sensitivity analysis of the soil permittivity in a reasonable range for frozen ground instead of a fix number of 3.6 + 0.9i.

We agree that the soil contribution in the lower frequency limit can be significant. However, we used a value derived from a study (Rautiainen et al., 2012) which was dedicated to derive soil permittivity, which lies in the range of previously published values. Our approach was not to treat the soil permittivity as optimization parameter, as for the soil type in Sodankylä measurements (e.g. Hallikainen et al., 1985) and retrievals (e.g. Rautiainen et al., 2012) for the permittivity were available.

3. In the model results, the vv is always slightly higher than hh. However, the SnowScat data shows more variability of the vv/hh ratio. Please provide some insights for both model results and data analysis.

We attributed the high variability in the SnowScat signal in general to the heterogeneity of the ground and snowcover at the test site (see also Referee 1, comment on page 2622, lines 3-5). In

particular Figure 9 and 10 show a variable backscatter signal measured by SnowScat when the incidence angle and therefore the measurement location is changed. The model runs, however, were only preformed for one pit and cannot contain variability. The effect of the spatial variability on microwave emission is demonstrated in Figure 14 and section 4.2.3. However, a more detailed discussion of the variability of the vv/hh ration was not a particular subject of the paper.

4. In the figure 1, it will be more clear to mark the rs, rd in the plot as well as the sigma0, sigma_d from both snow-air and snow-ground interface.

We agree and included the parameters in Figure 1 and modified the caption accordingly:
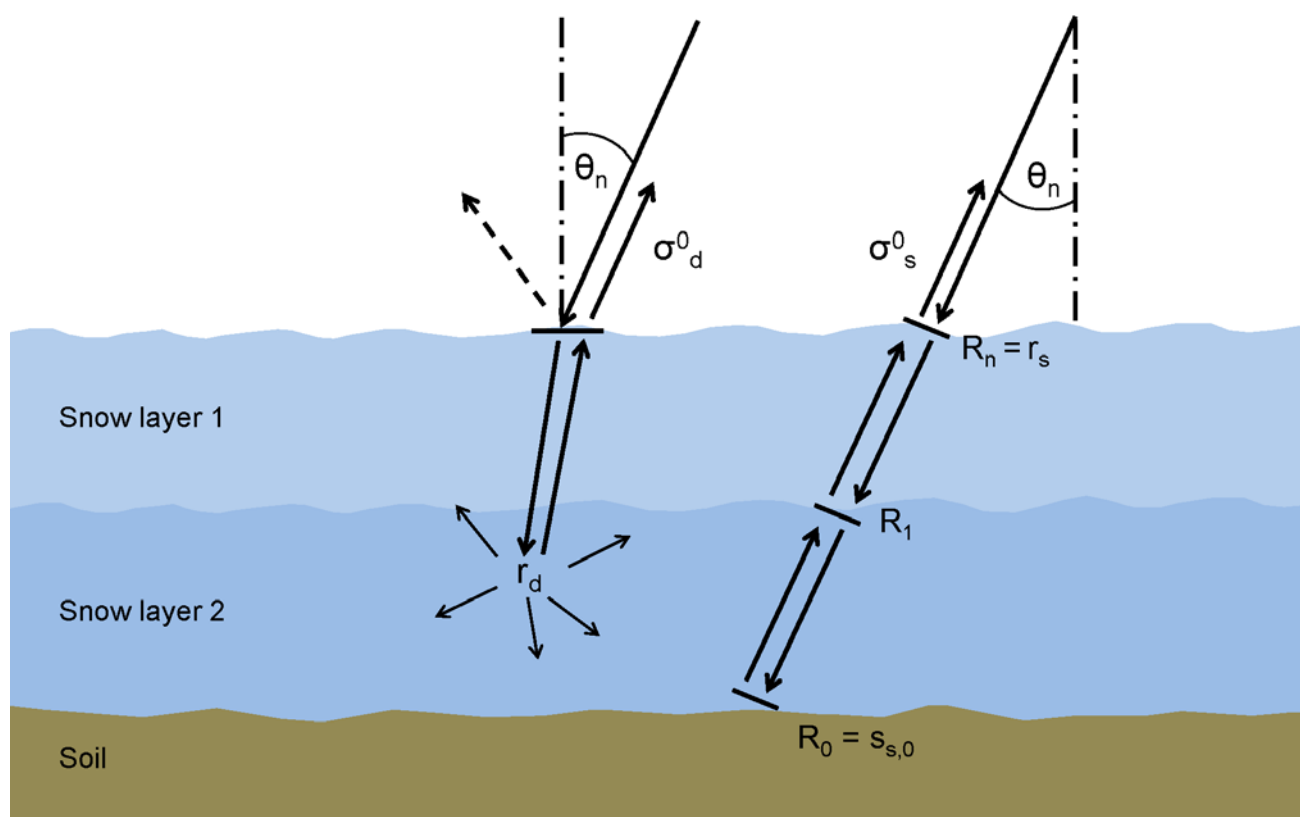
θ_n σ^0_d σ^0_s θ_n

$R_n = r_s$

Snow layer 1

R_1

r_d

Snow layer 2

$R_0 = s_{s,0}$

Soil

Snowpack (blue) with slightly undulated snow surface and layers.Waves incident at nadir angle θ_n are refracted at the snow surface followed by volume scattering with backscatter σ_0d (left); Specular backscatter σ _0 s from a slightly tilted patch of the surface, soil and layer interfaces (right). Diffuse r_d and specular reflectivities r_s = R_n, R_0 and R_1 are indicated.

5. In the backscattering plot, figure(7-13), it's more common to use dB as the unit for backscattering. I suggest to convert the y-axis into dB scale for better illustration and cross-comparison with other papers.

In order to relate the data to radiometry we used a linear scale. However, we agree that the cross-comparison to other paper is enhanced by using dB but in this study we only focused on the performance of the model and not on an intercomparison of models.

6. In equation (9), what is sigma_n refer to?

We could not find sigma_n in eq.9.
θ_n is the zenith angle, with μ_n = cos (θ_n), as defined on page 2610 line 21.

References:

Hallikainen, M., Ulaby, F., Dobson, M., El-Rayes, M., and Wu, L.: Microwave dielectric behavior of wet soil – Part 1: Empirical models and experimental observations, IEEE T. Geosci. Remote, 23, 25–34, 1985

Löwe, H., Spiegel, J. K., and Schneebeli, M.: Interfacial and structural relaxations of snow under isothermal conditions, J. Glaciol., 57, 499–510, doi:10.3189/002214311796905569, 2011

Rautiainen, K., Lemmetyinen, J., Pulliainen, J., Vehviläinen, Drusch, M., Kontu, A., Kainulainen, J., and Seppänen, J.: L-band radiometer observations of soil processes in boreal and subarctic environments, IEEE T. Geosci. Remote, 50, 1483–1497, 2012

Torquato, S.: Random Heterogeneous Materials, Springer, New York, 2002

MEMLS3&a: Microwave Emission Model of Layered Snowpacks adapted to include backscattering

M. Proksch[1,5]**, C. Mätzler**[2,6]**, A. Wiesmann**[2]**, J. Lemmetyinen**[3]**, M. Schwank**[2,4]**, H. Löwe**[1]**, and M. Schneebeli**[1]

[1]WSL Institute for Snow and Avalanche Research SLF, Flüelastrasse 11, 7260 Davos Dorf, Switzerland
[2]GAMMA Remote Sensing Research and Consulting AG, Worbstrasse 225, 3073 Gümlingen, Switzerland
[3]Arctic Reserach Center, Finnish Meteorological Institute FMI, 00101 Helsinki, Finland
[4]Swiss Federal Institute for Forest, Snow and Landscape Research WSL, Zürcherstrasse 111, 8903 Birmensdorf, Switzerland
[5]Institute of Meteorology and Geophysics, University of Innsbruck, Innrain 52, 6020 Innsbruck, Austria
[6]Institute of Applied Physics, University of Bern, Sidlerstrasse 5, 3012 Bern, Switzerland

Correspondence to: M. Proksch (proksch@slf.ch)

Abstract

The Microwave Emission Model of Layered Snowpacks (MEMLS) was originally developed for microwave emissions of snowpacks in the frequency range 5–100 GHz. It is based on six-flux theory to describe radiative transfer in snow including absorption, multiple volume scattering, radiation trapping due to internal reflection and a combination of coherent and incoherent superposition of reflections between horizontal layer interfaces. Here we introduce MEMLS3&a, an extension of MEMLS, which includes a backscatter model for active microwave remote sensing of snow. The reflectivity is decomposed into diffuse and specular components. Slight undulations of the snow surface are taken into account. The treatment of like and cross polarization is accomplished by an empirical splitting parameter q. MEMLS3&a (as well as MEMLS) is set up in a way that snow input parameters can be derived by objective measurement methods which avoids fitting procedures of the scattering efficiency of snow, required by several other models. For the validation of the model we have used a combination of active and passive measurements from the NoSREx campaign in Sodankylä, Finland. We find a reasonable agreement between the measurements and simulations, subject to uncertainties in hitherto unmeasured input parameters of the backscatter model. The model is written in MATLAB and the code is publicly available for download through the following website: http://www.iapmw.unibe.ch/research/projects/snowtools/memls.html.

1 Introduction

Empirical observations reveal a wide range of different microwave signatures in active or passive remote sensing over snow covered areas as shown e.g. by Mätzler (1987). The lack of realistic models to understand these signatures was the motivation for efforts leading to the Microwave Emission Model of Layered Snowpacks (MEMLS) in the 1990s (Mätzler, 1996; Wiesmann and Mätzler, 1999). Initially the microwave emission behavior of single snow layers was investigated by Weise (1996) and later by Wiesmann (1997). The measurements led to an empirical approach for the scattering coefficient of snow in the frequency range 5–100 GHz

2

and correlation-length range 0.05–0.3 mm (Wiesmann et al., 1998) and to a first version of MEMLS (Wiesmann and Mätzler, 1999). Empirical relations for the scattering coefficient have also been implemented in the Helsinki University of Technology HUT model developed by Pulliainen et al. (1999) and later adapted by Lemmetyinen et al. (2010). MEMLS was extended to coarse grained snow for correlation lengths up to 0.6 mm (Mätzler and Wiesmann, 1999). The snow microstructure was characterized by an exponential correlation function which allows to compute the scattering coefficient analytically using the Improved Born Approximation (IBA) (Mätzler, 1998).

As an advantage of IBA and the characterization of snow in terms of correlation functions, the most relevant snow input parameters of MEMLS, correlation length and density, can be measured directly and objectively by various methods. Other models may require e.g. a conversion of measured parameters to model-effective ones (Kontu and Pulliainen, 2010; Lemmetyinen et al., 2015). The exponential correlation length could be e.g. obtained by micro-computed tomography (μCT) (Schneebeli and Sokratov, 2004) from a fit to the reconstructed three-dimensional microstructure (Löwe et al., 2013). Snow density and correlation length can be also obtained efficiently from field measurements (Proksch et al., 2015), using high resolution penetrometry (SMP) (Schneebeli and Johnson, 1998). Alternatively, optical methods can be used, e.g. Matzl and Schneebeli (2006); Gallet et al. (2009); Arnaud and Picard (2011), to measure the Specific Surface Area (SSA) and use an empirical relation to compute the exponential correlation length (Mätzler, 2002). The latter method is appealing since SSA is commonly available. Accordingly MEMLS was widely used for various questions related to passive microwave remote sensing (Durand et al., 2008; Rees et al., 2010; Toure et al., 2011; Langlois et al., 2012; Schwank et al., 2014).

In recent years, there was an increasing interest of the snow remote sensing community in active microwave measurements, which was mainly driven by the Cold Regions Hydrology High-Resolution Observatory CoReH$_2$O (Rott et al., 2010) and related activities. However, single layer models for the radar signal as presented in Rott et al. (2010) or Ulaby et al. (1984) are mainly used for efficient operation in retrieval schemes. For the sake of low complexity, these models are naturally based on strongly simplifying assumptions, e.g. treating snow as a col-

lection of independent scatterers. However, scatterers are densely packed in snow and strongly interact with each other. More realistic models based on dense media radiative transfer (DMRT) have been developed (Tsang et al., 2007; Chang et al., 2014), including the possibility of using the numerical solution of Maxwell's equations for the single layer scattering coefficients (Ding et al., 2010; Xu, 2012). The DMRT-based models however require at least two microstructural input parameters, which can be presently obtained only by μCT and often require time consuming casting procedures in the field.

To cope with recent requirements in active microwave remote sensing, while relying on an established, physical model of intermediate complexity, it is the aim of the present paper to extend MEMLS and develop a first version of MEMLS3&a. Thereby we can build on the description of the microstructure in terms of the exponential correlation length as a single, objective parameter which can be derived from in-situ field measurements. For the backscattering model, we shall extend the description of the snowpack in MEMLS to account for a slightly undulated snow surface as shown in Fig. 1. The slightly undulated patches should be small enough to leave the emission largely unaffected, but large enough to allow specular backscattering at near-vertical incidence.

The paper is organized as follows: in Sect. 2 we present the development of the model and the calculation of the total backscatter with its specular and diffuse components. In Sect. 3 the validation data consisting of active and passive microwave measurements from Sodankylä, Finland is described. Section 4 presents the validation of both MEMLS and MEMLS3&a using the Sodankylä data, followed by a discussion (Sect. 5) and the conclusions (Sect. 6). Details about the calculation of the specular reflectivity are given in the Appendix.

2 Model development

In MEMLS the snow cover is considered as a stack of *n* horizontal layers with planar boundaries at the snow surface and between snow layers. Each layer is characterized by snow parameters (layer thickness, correlation length, density, liquid water content and temperature) that determine the layer-radiative properties. Also the salinity can be taken into account layerwise. The

4

snow-ground interface is characterized by a reflectivity s_0. A sandwich model is used to combine internal scattering and reflections at the interfaces. Internal volume scattering is accounted by a two-flux model (up- and downwelling streams) derived from a six-flux approach (fluxes in all space directions). The absorption and scattering coefficients are functions of the six-flux parameters. The absorption coefficient can be obtained from density, frequency, temperature and salinity; the scattering coefficient depends on the correlation length, density and frequency. For a detailed description of MEMLS we refer to the technical documentation (Mätzler and Wiesmann, 2012). In the following, we focus on the backscatter model by considering the total backscatter as a sum of specular and diffuse components. Since the total reflectivity of a snowpack is related to its emissivity, it can be derived from passive observations alone. Thereby active and passive observables can be appropriately combined to obtain a prediction for the radar backscatter.

2.1 Link between active and passive observables

At any given frequency and polarization of electromagnetic radiation with incident direction (μ_n, ϕ_n) defined by zenith angle θ_n (where $\mu_n = \cos\theta_n$) and azimuth angle ϕ_n at the snow-air interface (cf. Fig. 1), the reflectivity r of the surface is related to its emissivity e (in the reciprocal direction) by Kirchhoff's Law

$$r = 1 - e \tag{1}$$

For a more general description of Kirchhoff's Law, see Mätzler and Melsheimer (2006). Equation (1) relates the emissivity, the key quantity of passive microwaves, to the reflectivity, a quantity linked to scattering. It is this relation that allows us to link active and passive microwave remote sensing. The reflectivity represents the fraction of the incident radiation that is scattered in the hemisphere above the surface. If the scattered radiation is diffuse (Lambertian reflectance) we can estimate the fraction in the backscatter direction. Furthermore, with information about the statistics of surface slopes, we can determine the contribution of backscatter arising from specular reflection at surface facets that are normal to the incident direction. Therefore we will represent the total reflectivity as a sum of diffuse and specular components. The reflectivity can

be represented as an integral over scattering directions in the upper hemisphere of the bistatic scattering function S

$$r = \frac{1}{4\pi\mu_n} \int\limits_{2\pi} S(\mu_n, \phi_n, \mu, \phi)\mathrm{d}\Omega = \frac{1}{2\mu_n} \int\limits_0^1 S(\mu_n, \mu)\mathrm{d}\mu \qquad (2)$$

Here $\mathrm{d}\Omega = \mathrm{d}\mu\mathrm{d}\phi$ is the infinitesimal solid-angle element in the scattered direction. The azimuth integration extends from 0 to 2π, and the last expression is valid for azimuth-independent functions. The function S describes the scattering from incident direction (μ_n, ϕ_n) to the scattering direction (μ, ϕ). Thus, backscattering is determined by $S(\mu_n, \phi_n, \mu_n, \phi_n)$. Chandrasekhar (1960) introduced the S function in his monograph on radiative transfer. He showed that S is reciprocal

$$S(\mu_n, \phi_n, \mu, \phi) = S(\mu, \phi, \mu_n, \phi_n) \qquad (3)$$

Furthermore S is identical to the bistatic scattering cross section σ^0 introduced by Ulaby et al. (1981), see their Eqs. (4.186) and (4.187), more exactly to the sum of the like- and crosspolarization terms, $S = \sigma^0_{\mathrm{like}}(\theta_n, \phi_n, \theta, \phi) + \sigma^0_{\mathrm{cross}}(\theta_n, \phi_n, \theta, \phi)$. It is also related to Peake's (1959) function $\gamma = S/\mu_n$, i.e. the $1/\mu_n$ factor of Eq. (2) is included inside this function. For completeness we note that S is related to, but differs from other definitions: the reflection function R used for instance by Kokhanovsky (2001) differs by a factor π from the Bidirectional Reflection Distribution Function (BRDF) used in optical remote sensing (Kasten and Raschke, 1974), and all quantities are related by

$$\begin{aligned} S(\mu_n, \phi_n, \mu, \phi) &= \mu_n\gamma(\mu_n, \phi_n, \mu, \phi) \\ &= 4\mu_n\mu\, R(\mu_n, \phi_n, \mu, \phi) = 4\pi\mu_n\mu\, \mathrm{BRDF}(\mu_n, \phi_n, \mu, \phi) \end{aligned} \qquad (4)$$

The S function can be highly complex. However, for diffuse scattering, some empirical functions are provided in the literature, see e.g. Mätzler and Rosenkranz (2007), the simplest one for Lambert scattering

$$S_\mathrm{d} = S_0\mu_n\mu \qquad (5)$$

6

where the subscript d indicates diffuse scattering, and S_0 is a constant. By integration according to Eq. (2), we find that the diffuse reflectivity r_d is independent of the incidence angle, namely $r_d = S_0/4 = R$, and thus equal to Kokhanovsky's R. The normalized backscattering cross section is given by $\sigma_d^0 = S_d(\mu = \mu_d)$, which can be expressed by r_d via

$$\sigma_d^0 = 4r_d\mu_n^2 \tag{6}$$

Indeed, Lambertian behaviour was found by the investigation of the HPACK Model for snow by Mätzler (2000). It is an extension of an earlier one-layer, active-passive model of Tsang et al. (1982) to include multiple-isotropic scattering in the snow as well as refraction and reflection at the snow surface. The combined effect led to Lambert scattering for the diffuse component.

Unspecified in Eq. (6) is the separation of σ_d^0 in its like- and cross-polarized components. For isotropic scatterers considered in HPACK, the first-order backscattering is like polarized, and cross polarization requires higher-order scattering. However, the structure of natural snow is highly complex, meaning that cross polarization occurs for all scattering orders. Therefore we introduce an empirical relationship with a splitting parameter q which defines the cross-polarized part, whereas $(1 - q)$ represents the like-polarized fraction, via

$$\sigma_{d,pp'}^0 = \begin{cases} (1-q)\sigma_{d,v}^0, & p = p' = v \\ (1-q)\sigma_{d,h}^0, & p = p' = h \\ q\left(\sigma_{d,v}^0 + \sigma_{d,h}^0\right)/2, & p = v, p' = h; \text{ or } p = h, p' = v \end{cases} \tag{7}$$

Here we took into account that r_d and thus σ_d^0 are slightly different for horizontal (h) and vertical (v) polarization. Now, Eq. (6) can be rewritten using the polarization terms for incident waves at vertical and horizontal polarization, respectively:

$$\sigma_{d,v}^0 = \sigma_{d,vv}^0 + \sigma_{d,hv}^0 = 4r_{d,v}\mu_n^2$$
$$\sigma_{d,h}^0 = \sigma_{d,hh}^0 + \sigma_{d,vh}^0 = 4r_{d,h}\mu_n^2 \tag{8}$$

An additional contribution to backscattering results from specular reflection as shown in Fig. 1. By considering only slight undulations, specular backscattering is limited to near-vertical inci-

dence. For a Gaussian distribution of surface slopes, the backscattering coefficient of the specular term can be written as

$$\sigma_{\mathrm{s}}^0 = r_{\mathrm{s},0} \frac{\exp\left[-\tan^2\theta_n/(2m^2)\right]}{2m^2\mu_n^4} \tag{9}$$

where m^2 is the mean-square slope, and $r_{\mathrm{s},0}$ refers to r_{s} at normal incidence (Fig. 1, right). This equation corresponds to the ~~physical-optics and to the~~ geometrical-optics solution for undulating surfaces, see Ulaby et al. (1982, Eqs. 12.45 and 12.46), and Kong (1986, Sect. 6.6). Here we generalize it from surface scattering to specular terms that fit the observation geometry (i.e. specular reflectivity for local normal incidence angle). Furthermore we note that Eq. (9) describes like-polarized backscatter. For negligible anisotropy in the local surface plane the same values are obtained for hh and vv polarization, and the cross-polarization terms are zero.

For both v and h polarization the total reflectivity is the sum of the diffuse and the specular component:

$$r = r_{\mathrm{d}} + r_{\mathrm{s}} \tag{10}$$

While Eqs. (6) and (8) are valid for r_{d}, Equation (9) applies to r_{s}, but taken at normal incidence. With some additional effort described below, MEMLS provides both, r_{d} and r_{s} and the total backscattering coefficient as the sum:

$$\sigma^0 = \sigma_{\mathrm{d}}^0 + \sigma_{\mathrm{s}}^0 \tag{11}$$

2.2 Determination of r

Apart from the physical temperatures of all snow layers including the ground temperature, also the downwelling sky brightness temperature T_{sky} must be provided as input in MEMLS. The output is the brightness temperature T_{b} that is observed as upwelling radiation above the snowpack

$$T_{\mathrm{b}} = r T_{\mathrm{sky}} + (1-r)T_{\mathrm{eff}} \tag{12}$$

8

Here T_{eff} is the emission-effective temperature of snow and ground. The reflectivity r can thus be computed via T_{b} (T_{b1}, T_{b2}) from two arbitrary, but different values of T_{sky} (T_{sky1}, T_{sky2}), such as 100 and 0 K. The reflectivity then follows from

$$r = \frac{T_{\text{b1}} - T_{\text{b2}}}{T_{\text{sky1}} - T_{\text{sky2}}} \tag{13}$$

2.3 Determination of r_{s}

According to Fig. 1 we need the specular reflectivities $r_{\text{s,v}}$ and $r_{\text{s,h}}$ at vertical and horizontal polarization at the observation incidence angle as well as $r_{\text{s,0}}$ at normal incidence. For brevity we omit subscripts indicating the polarization and just write r_{s} instead of $r_{\text{s,v}}$ and $r_{\text{s,h}}$. In many situations r_{s} can be identified by the reflectivity of the snow surface. This is especially true for wet snow and for snowpacks that consist of a single layer. However, if an old snowpack is covered by fresh snow, the dominant specular layer may be the interface between the fresh and the old snow. Also ice lenses form dominant reflectors inside the snowpack. Therefore MEMLS requires a method that estimates incoherent specular reflectivities for arbitrary stratifications. This derivation is detailed in the Appendix. As a result, if all layer interfaces are assumed to be smooth and the corresponding interface reflectivities s_j are determined by Fresnel's equations, the specular reflectivity R_j resulting from layers below z_j can be expressed in terms of a recurrence relation

$$R_j = s_j + \frac{[(1 - s_j)u_j]^2 R_{j-1}}{1 - u_j^2 s_j R_{j-1}}, \quad j = 1, \dots n \tag{14}$$

where s_j is the interface reflectivity on top of layer j and $u_j = \exp(-\gamma_{\text{e},j} d_j / \mu_{j-1})$ is the coherent transmissivity of Layer j (Fig. 2). The extinction coefficient is denoted by $\gamma_{\text{e},j}$ and d_j is the layer thickness. The specular reflectivity of the entire snowpack-ground system then is given by

$$r_{\text{s}} = R_n \tag{15}$$

9

Equation (14) starts with $j = 1$ at the ground as the lowest layer contributing to specular reflection. In contrast to the smooth interfaces assumed between snow layers, the ground is regarded as a rough surface and its reflectivity is additively decomposed into a diffuse and a specular part according to $s_0 = s_{s,0} + s_{d,0}$. Accordingly, the ground reflectivity $R_0 = s_{s,0}$ constitutes the initial condition for the recurrence relation (14).

2.4 Synopsis of the backscatter model

Finally, we briefly recap how specular and diffuse components from the previous section are practically reassembled in MEMLS3&a for the computation of the total backscatter:

1. The total backscatter σ^0 is divided into a specular and diffuse component, σ_s^0 and σ_d^0, respectively (cf. Eq. 11).

2. The specular component σ_s^0 is derived from Eq. (9) and arises from the rough soil surface (via $s_{s,0}$) and the layer interfaces and snow-air interface, which are both assumed to be slightly undulated.

3. The diffuse component of the backscatter σ_d^0 is derived from the diffuse component r_d of the total reflectivity (Eq. 6), which requires the calculation of the total reflectivity r (Eq. 13) and its specular component r_s (Eqs. 14 and 15).

Thus the model accounts for multiple scattering at the undulated layer interfaces. The diffuse scattered radiation is assumed to be Lambertian which allows to estimate the fraction scattered in the backscatter direction. More complex processes such as coherent backscatter enhancement recently presented by Tan et al. (2015) are currently not considered in MEMLS3&a.

2.5 Primary input parameters

For a simulation run at a given frequency f, polarization p and observation incidence angle θ_n all snow physical parameters described in Table 1 are required for each snow layer ($j = 1, 2, \ldots, n$). From these primary input parameters secondary parameters are computed as described in the previous version of MEMLS (Wiesmann and Mätzler, 1999).

3 Validation data

We used snow input data generated from three different snow measurement methods to run model simulations which are compared to backscatter measurements from ESA's SnowScat scatterometer for validation (Werner et al., 2010). All measurements were made on 1 March 2012 at the test site of the Finnish Meteorological Institute (FMI), in Sodankylä, Finland, during ESA's Nordic Snow and Radar Experiment (NoSREx) III (Lemmetyinen et al., 2013). The snow measurements were conducted directly in the field of view of the scatterometer and the radiometer, in order to minimize the influence of the spatial variability of the snowpack.

3.1 Test site

In the NoSREx campaign, the SnowScat scatterometer and SodRad radiometers were installed on two platforms overlooking a forest clearing. For the NoSREx measurements, SnowScat was set to measure several incidence angles over a wide sector. For the purpose of the present work both SnowScat and SodRad were turned in azimuth to point towards the same location on the snowpack, where a destructive snowpit measurement was made after the microwave measurements were completed.

The soil composition under the snowpack is dominantly mineral soil, with a thin vegetation layer on the surface (ca. 5 cm). A survey conducted in 2010 gave the soil composition beneath the vegetation layer as 70 % sand, 1 % clay and 29 % silt. Trees and shrubs higher than 10 cm were removed from the site prior to measurements. The surface vegetation consists of low lichen, moss and heather (Fig. 15).

3.2 SnowScat

The validation data was measured with ESA's SnowScat instrument (Werner et al., 2010) developed by Gamma remote sensing, Gümlingen, Switzerland. It is an X-to Ku-Band fully polarimetric step-frequency radar with an internal calibration loop which measures at a frequency range of 9.2 to 17.8 GHz, with a frequency resolution of 3.072 MHz. Data are presented for

three sub bands with center frequencies of 10.2, 13.3 and 16.7 GHz with 2 GHz bandwidth. The -3 dB beam-width of the horn-antennas are 5 and 12°, depending on frequency and polarization. An aluminum sphere is used as calibration target to correct for long term drifts. The instrument is mounted on a 9 m high tower and is able to rotate around azimuth-direction and to vary the incidence angle. For the validation data used in this study, SnowScat was pointed directly at the location where the in-situ measurements were conducted. The instrument was then operated at an incidence angle of 50°.

3.3 SodRad

The SodRad (Sodankylä Radiometer) system was mounted on a 4.1 m-high platform. In 2012 measurements at 10.65, 18.7, 21 and 37 GHz (H and V pol) were available from the system. The radiometers were calibrated using a two-point calibration with external targets before the start of the campaign. Verification of calibration stability was performed using periodic observations of the sky at zenith. Absolute accuracy of the calibration was estimated to be better than 1 K for the 18.7, 21 and 36.5 GHz channels, and better than 2 K for the 10.65 GHz channel. The beam width of all channels was 6°. The fields-of-view of the radiometers were clear of all standing vegetation.

4 Validation results

4.1 Model initialization

4.1.1 Snow input parameters

The most crucial snow input parameters required to drive MEMLS3&a are density and correlation length. We derived these parameters from three different snow measurement methods in order to illustrate different ways of acquisition (Fig. 4). First, density and correlation length were derived according to Löwe et al. (2011), using three-dimensional reconstruction by μCT (Schneebeli and Sokratov, 2004) of snow samples cast in the field. The sample casting tech-

nique is described in detail by Heggli et al. (2009). Second, we used the SnowMicroPen (SMP, Schneebeli and Johnson, 1998), a high resolution penetrometer. The derivation of density and correlation length from the SMP is detailed in Proksch et al. (2015). Finally, the near-infrared photography NIP, developed by Matzl and Schneebeli (2006), allows the measurement of the Specific Surface Area (SSA) of snow which is used to define the length scale

$$l_c = \frac{4(1 - \rho_{snow}/\rho_{ice})}{SSA} \tag{16}$$

The exponential correlation length l_{ex} is then obtained from the empirical relation

$$l_{ex} = 0.75 \, l_c \tag{17}$$

put forward by Mätzler (2002).

As NIP does not provide the snow density, it was measured using a standard $100 \, \text{cm}^3$ density cutter with a vertical sampling interval of $4 \, \text{cm}$. A more detailed comparison of snow measurement methods with respect to microwave remote sensing can be found in Proksch and Schneebeli (2012). The density and correlation length profiles derived by the different methods are shown in Figs. 5 and 6. The different methods are in general in agreement, besides the correlation length derived from NIP, which shows very large values in the lowest layer, which is an artifact of the preparation process of the profile wall. The snow temperature was assumed to be constant at $-3\,^\circ\text{C}$. At this temperature the snow is dry and does not contain liquid water. The density and correlation length profiles were averaged to a vertical resolution of $3 \, \text{cm}$ to avoid any effects of coherent layers for the wavelength considered by SnowScat.

4.1.2 Soil contribution

Besides the snow input parameters, the snow-ground reflectivity s_0 is required. Since direct measurements were not possible due to the presence of the snow cover, this parameter has to be modeled. Here we used the empirical model of Wegmüller and Mätzler (1999), which was previously used in various studies (e.g. Lemmetyinen et al., 2010; Takala et al., 2011;

Rautiainen et al., 2012; Kontu et al., 2014). We used a value for the complex soil permittiviy of frozen ground of $\epsilon_g = 3.6 + 0.9i$ in line with Rautiainen et al. (2012), and set the standard deviation of the soil surface height rms_g under the vegetation to 5 mm.

To account for the correct incidence angle at the snow-ground interface, the following auxiliary procedure is carried out for each model run. First, MEMLS3&a is run with $s_0 = 0$ and the incidence angle at the snow-ground interface is determined. Second, this angle was used in the model of Wegmüller and Mätzler (1999) to calculate s_0 which was then used to run MEMLS3&a again, now accounting for the correct incidence angle on the snow-ground interface. The resulting values for s_0 ranged from 0.025 for 18 GHz at V-pol to 0.037 for 10 GHz at H-pol.

The model of Wegmüller and Mätzler (1999) gives the total reflectivity of the snow-ground interface. To determine its specular component s_{s0}, we assumed s_{s0} to be proportional to s_0. A constant factor of 0.75 ($s_{s0} = 0.75s_0$, for all polarizations and frequencies) was chosen to match SnowScat measurements with our simulations.

The soil temperature was measured to be $-2.5\,°C$. For the comparison to SnowScat observation, the cross polarization fraction q was chosen to match the microwave measurements, which led to $q = 0.15$. The mean slope of surface undulations m has no influence for an incidence angle of $50°$ if values are smaller than 0.25. We choose $m = 0.1$ for our simulations. The sensitivity to both parameters will be discussed in Sect. 4.2.2.

4.1.3 Sky temperature

A further input to the model is the downwelling brightness temperature T_{sky} of the sky. As SnowScat did not measure T_{sky}, we estimated T_{sky} from the SodRad radiometer which measures the sky brightness temperature $T_{sky,z}$ at zenith. To fit our frequency interval of 10–18 GHz used for the simulation, we linearly interpolated $T_{sky,z}$ values to match the interval. To convert $T_{sky,z}$ to an effective sky brightness temperature T_{sky} which is representative for the whole scenery at the main test site, we first determined the sky opacity τ_z at zenith from $T_{sky,z}$ (similar to Mätzler,

14

1994, Eq. 7)

$$\tau_z = -\ln\left(\frac{T_{\text{sky,z}} - T_{\text{air}}}{T_{\text{back}} - T_{\text{air}}}\right) \tag{18}$$

where $T_{\text{air}} = 270\,\text{K}$ is the air temperature and $T_{\text{back}} = 2.7\,\text{K}$ is the background radiation. A good approximation for the effective opacity τ_{eff} representative for the whole scenery is given by

$$\tau_{\text{eff}} = 2\,\tau_z \tag{19}$$

as shown by Mätzler (2005). The sky brightness temperature is finally computed from

$$T_{\text{sky}} = 2.7e^{-\tau_{\text{eff}}} + (1 - e^{-\tau_{\text{eff}}})T_{\text{air}} \tag{20}$$

4.2 Results

4.2.1 Simulation results

We choose the scattering option of the improved Born approximation (Mätzler, 1998) to run the model. For the soil, snow and T_{sky} parameter settings described in Sect. 4.1, the results for MEMLS3&a driven by SMP, CT and NIP input data are shown in Fig. 7 for an incidence angle of $50°$. CT and SMP input results in good agreement between model and measurement, with a mean absolute error (MAE) of 4.0×10^{-3} and 4.3×10^{-3} for vv polarization, 3.2×10^{-3} and 1.6×10^{-3} for hh polarization and 4.0×10^{-4} and 5.3×10^{-4} for hv polarization for CT and SMP input, respectively. NIP input leads to an overestimation of σ_0, which emerges from the NIP artefact towards the bottom of the profile (Sect. 4.1.1) where the correlation length values are too large. However, MEMLS3&a driven with CT input data is in good agreement with SnowScat measurements (Fig. 8).

The dependence on the incidence angle at 10.2 and 16.7 GHz is shown in Figs. 9 and 10. MEMLS3&a is in general agreement with SnowScat, with a MEA of 2.3×10^{-3} and 9.6×10^{-3} for vv polarization, 2.1×10^{-3} and 1.2×10^{-2} for hh polarization and 6.3×10^{-4} and 2.6×10^{-3} for hv polarization at 10.2 GHz and 16.7 GHz, respectively. The polarization difference is

15

slightly too small at 16.7 GHz. The SnowScat observations at different incidence angles show a certain amount of scatter, which we attribute to the ~~limited number of independent looks (< 40)~~ heterogeneity of the ground and snowcover at the test site.

4.2.2 Sensitivity analysis

In this section the sensitivity of MEMLS3&a to s_{s0} as well as to the two empirical parameters, the cross-polarization ratio q and the root-mean-square slope of surface undulations m are shown. For clarity, we restrict ourselves to those MEMLS3& a runs which were driven with CT input data and the best fit values mentioned above ($q = 0.15$, $m = 0.1$, $s_{s0} = 0.75 s_0$ for both polarizations), if not indicated differently.

The specular snow-ground reflectivity s_{s0} is a crucial parameter for the simulation because a higher specular snow-ground reflectivity leads to lower backscatter. This effect is larger at low frequencies due to the lower attenuation of electromagnetic radiation in snow. Figure 11 shows that σ^0 is significantly increased with decreasing s_{s0} values and vice versa, more pronounced at low frequencies.

The empirical cross-polarization ratio q is the fraction of cross-polarized backscatter: increasing q lowers co-polarization and increases cross-polarization by the same magnitude (cf. Eq. 7). Figure 12 illustrates this by two values of q (0.15 and 0.3, respectively).

~~The effect~~ A larger value of m ~~is limited to~~ represents a stronger undulated surface and increases the spectral component of the backscatter, in particular at small incidence angles~~(.~~ Fig. 13 ~~). It diminishes completely for~~ shows this behavior, with increasing backscatter for increasing values of m and decreasing incidence angles. Given values smaller than 0.1, m has no effect at incidence angles larger than 25~~and is not present for cross polarization~~°. Further, cross polarization is in general not affected by m. Note that these results are only valid for the given snow and soil conditions, i.e. the sensitivity of parameters might change in different environmental conditions.

4.2.3 Comparison with passive simulations

To prove the concept of the MEMLS architecture, which is the fundament for MEMLS3&a, we compare our active simulations with passive simulations using the same input data (Sect. 4.1). The validation data was measured by the SodRad radiometer (Sect. 4.1.3). Similar to SnowScat, SodRad was also pointed to the location of the in-situ measurements (azimuth angle 140°). The instrument was operated at an incidence angle of 50°.

To run MEMLS, 15 SMP measurements inside the main test site in Sodankylä were used in order to capture the spatial variability of the snowpack. For each SMP measurement one MEMLS simulation was conducted. Figure 14 shows the results of the 15 MEMLS runs in combination with the SodRad measurements.

The agreement between model and observation generally decreased towards higher frequencies. At 36 GHz the average of all 15 MEMLS runs was at maximum 22 K too low for V-pol and 12 K too low for H-pol. Compared to the operational azimuth angle of 190°, the difference between model and observation decreased to 16 and 1 K for V-pol and H-pol, respectively. The differences at 10 GHz are comparably lower, with 5 K at maximum. The standard deviations of the 15 MEMLS runs, which are solely due to spatial variability of the snow, increased with frequency. At 36 GHz the standard deviation was around 8 K for both polarizations. The difference in azimuth angles of SodRad was even larger, with 12 K at 36 GHz H-pol. This underlines the influence of the spatial variability of the snowpack on modeled and measured brightness temperatures, which will be discussed in the next section. The agreement between model and observation should be always interpreted with respect to the variation in brightness temperatures caused by the spatial variability of the snowpack.

5 Discussion

As shown in the previous Sect. 4, MEMLS3&a simulations were in ~~good~~ reasonable agreement with SnowScat observations. To achieve this agreement, however, several parameters were chosen to match model and observation. This was necessary, since the active part contains, in

contrast to the passive part, empirical parameters (s_{s0}, q and m) which could not be measured. Likewise, the ground parameters s_0 and rms_g are subject to uncertainties.

The specular part of the snow-ground reflectivity s_{s0} was chosen to be proportional to s_0 and the same factor of 0.75 could be applied for all frequencies and polarizations to convert s_0 into s_{s0}. With $s_{s0} = 0.75 s_0$, the main part of the snow-ground reflectivity is specular. This requires the ground to be smooth and the overlaying snow layer to be transparent. The vegetation is subject to very low temperatures and a steady temperature gradient, which forces the water of the soft vegetation (lichen, mosses, shrubs (Myrtillus species), Fig. 15) to move upwards into the snow. Given the height of the vegetation of less than 10 cm it seems reasonable to assume that the vegetation dries out during winter and can be treated as fully transparent for the present microwave frequencies. This allows the soil interface to act as specular reflector, which is then accounted for by s_{s0} in the model. Though being reasonable, a sound justification of this line of argumentation requires further investigations.

The cross-polarization in MEMLS3&a is solely determined empirically via the parameter q. This pragmatic approach was chosen since the physical origin of cross-polarization in snow is still subject of ongoing research. In the DMRT based approach (Tsang et al., 2007), cross polarization emerges from non-spherical shapes of aggregated spheres clusters. A different route to cross-polarization can be taken via the Discrete Dipole Approximation DDA such as Von Lerber et al. (2006) or Xu (2012), which principally accounts for multiple reflections and polarizations inside a given snow volume. DDA requires the full three-dimensional description of the microstructure, which can be provided by μCT. A comparison to such a model could further elucidate the justification and the value of the parameter q.

Another parameter chosen empirically is the mean slope of surface undulations m. In principle, this parameter could be obtained from the analysis of the surface height, similar to what has been done in Löwe et al. (2007) and Manes et al. (2008) for fresh snow. In a simple reasoning, the mean squared slope m can be expressed as the ratio between the standard deviation of the surface height and the lateral correlation length of the height correlation function. According to Manes et al. (2008) m would then take a value of 0.14 for fresh snow which is in the same order of magnitude as applied in our simulations ($m = 0.1$). This small scale roughness of the

snow surface is not taken into account by the model, where only slight surface undulations are allowed.

The individual magnitudes of the specular and diffuse contributions are shown in Figure 16. Towards higher frequencies the diffuse component increases and outweighs the specular reflectivity from 12.5 GHz for v-pol and from 14.5 GHz for h-pol. Note that the magnitude of the specular component also depends on the undulation of the surface and therefore on the value of m. However, a pronounced impact of m is limited to small incidence angles (Fig. 13 and Section 4.2.2) for reasonable values of m (m ≈ 0.1).

In contrast to MEMLS3&a, MEMLS does not require free empirical parameters. In this regard we attribute the fact that MEMLS3&a matches the SnowScat observation better than MEMLS the SodRad observations to the additional free parameters in MEMLS3&a, foremost s_{s0} and q. However, also for the passive simulations parameters had to be chosen without direct experimental justification, namely s_0 and rms_g, which determine the contribution of the snow-ground interface. This contribution is dominant and critical in our frequency range, as dry snowpacks thinner than $\sim 1\,\mathrm{m}$ are highly transparent. Unfortunately, the knowledge about the scattering at the ground surface is limited. Therefore the snow ground reflectivity s_0 was modeled using the model of Wegmüller and Mätzler (1999). This model is an empirical parametrization of the Fresnel formula depending on the standard deviation of the soil surface height rms_g and the soil permittivites. For the soil permittivities, Hallikainen et al. (1985) provides experimental data and Mironov et al. (2010) an empirical model based on experimental data, but dielectric models for the permittivities of frozen soils are still under development. For rms_g of the soil below the snowpack no measurements were available. In addition, the model of Wegmüller and Mätzler (1999) does not account for vegetation, which is in our case consistent with the argument on transparency given above. We note that estimating the snow-ground reflectivity is critical for all microwave models, which was also concluded from recent experiments (Roy et al., 2013; Montpetit et al., 2013). However, at $10\,\mathrm{GHz}$, the frequency which is most influenced by the soil, MEMLS and SodRad were in good agreement.

In contrast, the mismatch between model and measurements was largest at $36\,\mathrm{GHz}$, which is most sensitive to details of the snow microstructure. MEMLS assumes an exponential fit of

the density correlation function of the snow microstructure. The exponential fit is a reasonable starting point, but small deviations can have a large influence on scattering. As detailed by Löwe et al. (2011), the correlation function of snow can take different shapes and its representation by means of a single correlation length might be inappropriate. Instead the Teubner-Strey form, a two-scale form for bicontinuous media might be more appropriate. The inclusion of other types of correlation functions into MEMLS is possible by adapting the calculation of the scattering coefficient. We thus believe that the present model provides a suitable test case to investigate the impact of more sophisticated representations of the snow microstructure.

We further tried to assess the influence of the spatial variability of the snowpack. The standard deviation obtained from the 15 MEMLS runs is 8 K at 36.5 GHz, H- and V-pol, implying a non-negligible influence of the location of the in-situ snow measurements on the modeled brightness temperatures.

We also found that the higher values measured by SodRad throughout the whole frequency range at H-pol for an azimuth angle of 140° indicate an effect of the surrounding environment, such as trees, which were closer to the field of view at this azimuth angle. The spatial variability of the snowpack together with the influence of the environment are potentially able to bias simulated and measured brightness temperatures.

The degree of complexity of existing models simulating microwave backscattering from snow range from single layer approaches (Rott et al., 2010) to numerical solutions of Maxwell's equations (Xu, 2012; Ding et al., 2010). In this context, we propose MEMLS3&a as a model of intermediate complexity. In contrast to the HUT model (Pulliainen et al., 1999; Lemmetyinen et al., 2010), which has comparable complexity, MEMLS avoids traditional grain size as input parameter, which is prone to uncertainties in the visual estimation method (Painter et al., 2007). The advantage of MEMLS3&a (as well as MEMLS) is the correlation length as microstructural quantity, which can be obtained from objective measurements without conversion and, given the SMP retrieval method, with high efficiency in the field.

Presently, models differ not only in the representation of snow microstructure, but also in the solution of the radiative transfer or the type of interfaces between the layers, which makes it difficult to attribute the discrepancies in model performance to a particular part of the model.

A comparison at least for the passive models by Tedesco and Kim (2006) showed that no model was able to reproduce all of the investigated microwave observations. For a detailed model assessment in view of future developments, various effects (spatial variability, snow microstructure, soil) must be isolated. A promising way are measurements of specifically prepared snow slabs, as already presented by Wiesmann et al. (1998). Together with complete 3-D microstructural information these types of idealized experiments will allow to minimize spatial variability, avoid the influence of the ground and compare different microstructural concepts for scattering coefficients. Together with available multi-layer models like MEMLS3&a, DMRT-ML (Picard et al., 2013) or the DMRT-QMS package (Chang et al., 2014) this will clarify our understanding of the processes involved in microwave emission and scattering of snow.

6 Conclusions

We adapted the Microwave Emission Model of Layered Snowpacks MEMLS to include backscattering and presented a detailed description of the relevant parameters and their derivation. The reflectivity was decomposed into diffuse and specular components, and the snowpack was allowed to be slightly undulated. This procedure could be applied to other passive microwave models as well. Model simulations were in ~~good~~ reasonable agreement with scatterometer observations, if the specular snow-ground reflectivity s_{s0} and the cross polarization ratio q were chosen accordingly. We found that the contribution of the snow-ground interface is a critical parameter, which needs further investigation. The empirical formulation of the cross polarization ratio q is a limitation with respect to other existing microwave models. MEMLS3&a offers a model of intermediate complexity, which avoids fitting procedures of the scattering efficiency of snow in combination with SMP or μCT measurements. This eliminates a main uncertainty of snow characterization in microwave remote sensing.

MEMLS3&a is integrated in the standard release of MEMLS as separate sub-routine. Both versions, active and passive are built on the same set of core functions.

Appendix: Specular reflectivity of the layered snowpack

The purpose of the appendix is to derive the specular part of the reflectivity of a layered snow-pack, in order to separate it from the diffuse part by subtraction from the total reflectivity using MEMLS. It is assumed here that all layer interfaces are smooth and parallel to the surface in order to produce specular reflection. Separation between diffuse and specular reflection is required in bistatic-scattering and in backscatter models.

We consider a plane-parallel snowpack used in MEMLS as shown in Fig. 2. The relevant quantities of an arbitrary layer j are shown in detail in Fig. 3. The layer is specified by a transmissivity u_j for the directed radiation. The transmissivity is given by

$$u_j = \exp(-\gamma_{e,j} d_j / \cos \theta_{j-1}) \tag{A1}$$

where $d_j = z_j - z_{j-1}$ is the thickness and $\gamma_{e,j}$ is the extinction coefficient of layer j, respectively. In addition, the layer interfaces are characterized by an interface reflectivity, where s_j denotes the reflectivity of the top interface of layer j. Assuming smooth interfaces we can apply the Fresnel formulas to compute s_j. The propagation angle θ_{j-1} in layer j is given by Snell's law of refraction. At the bottom of the snowpack, the reflectivity $s_0 = s_{s0} + s_{d0}$ consists of a specular s_{s0} and a diffuse s_{d0} component.

The aim of the following procedure is to derive an expression for the total specular reflectivity R_j which results from transmission and reflections in all layers below z_j. In order to compute the specular reflectivity we assume sufficiently large directional intensities such that thermal radiation can be neglected. Note that A_j, B_j, C_j and D_j are downwelling and upwelling intensities just above and below the boundaries of the respective snow layer. By virtue of Fig. 3 we

can derive the following equations relating the directional intensities at the boundaries

$$A_j = u_j C_j \tag{A2}$$
$$B_j = R_{j-1} A_j \tag{A3}$$
$$C_j = (1 - s_j) A_{j+1} + s_j D_j \tag{A4}$$
$$D_j = u_j B_j \tag{A5}$$
$$B_{j+1} = R_j A_{j+1} = (1 - s_j) D_j + s_j A_{j+1} \tag{A6}$$

Furthermore, at the bottom we have

$$R_0 = s_{s0} \tag{A7}$$

where s_{s0} is the specular part of the ground-snow interface reflectivity.

In order to solve these equations for R_j, we first eliminate the D_j and C_j in Eqs. (A4) and (A6) by using Eqs. (A2) and (A5). In this way we obtain

$$u_j(1 - s_j) A_{j+1} = A_j - u_j^2 s_j B_j \tag{A8}$$

and

$$B_{j+1} = (1 - s_j) u_j B_j + s_j A_{j+1} \tag{A9}$$

Dividing Eq. (A8) by A_j and Eq. (A9) by A_{j+1} we get, together with Eqs. (A6) and (A3)

$$u_j(1 - s_j) A_{j+1}/A_j = 1 - u_j^2 s_j R_{j-1} \tag{A10}$$

and

$$R_j = (1 - s_j) u_j R_{j-1} A_j / A_{j+1} + s_j \tag{A11}$$

Eliminating the ratio $A_{j+1}/A_j = (1 - u_j^2 s_j R_{j-1})/[u_j(1 - s_j)]$ in Eq. (A11) leads to

$$R_j = s_j + [(1 - s_j) u_j]^2 R_{j-1} / \left(1 - u_j^2 s_j R_{j-1}\right) \tag{A12}$$

23

Equation (A12) is a recurrence relation for the total specular reflectivity at the snow surface, $r_s = R_n$. The initial condition for the recurrence relation is given by the ground reflectivity in Eq. (A7).

The described procedure is applied for horizontal and vertical polarization, separately. For v polarization we call $R_n = r_{s,v}$, and for h polarization we call $R_n = r_{s,h}$. These are the specular parts of the total reflectivities, rv and rh of MEMLS. The diffuse components $r_{d,v}$ and $r_{d,h}$ are thus

$$r_{d,v} = r_v - r_{s,v}$$
$$r_{d,h} = r_h - r_{s,h} \tag{A13}$$

The diffuse components should be nearly the same at both polarizations. This property can be tested by computing $r_{d,v}$ and $r_{d,h}$ from Eqs. (10) and (13), by taking the total reflectivities from MEMLS and the specular reflectivities from the method described here.

Code availability

The model is written in Matlab and available to the public through the following website: http://www.iapmw.unibe.ch/research/projects/snowtools/memls.html.

References

Arnaud, L. and Picard, G.: Measurement of vertical profiles of snow specific surface area with a 1 cm resolution using infrared reflectance: instrument description and validation, J. Glaciol., 57, 17–29, doi:10.3189/002214311795306664, 2011.

Chandrasekhar, S.: Radiative Transfer, Dover Publ., New York, NY, 1960.

Chang, W., Tan, S., Lemmetyinen, J., Tsang, L., Xu, X., and Yueh, S.: Dense media radiative transfer applied to SnowScat and SnowSAR, IEEE J. Sel. Top. Appl., 7, 3811–3825, doi:10.1109/JSTARS.2014.2343519, 2014.

Denoth, A., Foglar, A., Weiland, P., Mätzler, C., and Aebischer, H.: A comparative study of instruments for measuring the liquid water content of snow, J. Appl. Phys., 56, 2154–2160, doi:10.1063/1.334215, 1984.

Ding, K.-H., Xu, X., and Tsang, L.: Electromagnetic scattering by bicontinuous random microstructures with discrete permittivities, IEEE T. Geosci. Remote, 48, 3139–3151, 2010.

Durand, M., Kim, E., and Margulis, S. A.: Quantifying uncertainty in modeling snow microwave radiance for a mountain snowpack at the point-scale, including stratigraphic effects, IEEE T. Geosci. Remote, 46, 1753–1767, doi:10.1109/TGRS.2008.916221, 2008.

Fierz, C., Armstrong, R., Durand, Y., Etchevers, P., Greene, E., McClung, D., Nishimura, K., Satyawali, P., and Sokratov, S. A.: The international classification for seasonal snow on the ground, HP-VII Technical Documents in Hydrology 83, IACS Contribution 1, UNESCO-IHP, Paris, 2009.

Gallet, J.-C., Domine, F., Zender, C. S., and Picard, G.: Measurement of the specific surface area of snow using infrared reflectance in an integrating sphere at 1310 and 1550 nm, The Cryosphere, 3, 167–182, doi:10.5194/tc-3-167-2009, 2009.

Hallikainen, M., Ulaby, F., Dobson, M., El-Rayes, M., and Wu, L.: Microwave dielectric behavior of wet soil – Part 1: Empirical models and experimental observations, IEEE T. Geosci. Remote, 23, 25–34, 1985.

Heggli, M., Frei, E., and Schneebeli, M.: Instruments and methods snow replica method for three-dimensional X-ray microtomographic imaging, J. Glaciol., 55, 631–639, doi:10.3189/002214309789470932, 2009.

Kasten, F. and Raschke, E.: Reflection and transmission terminology by analogy with scattering, Appl. Optics, 13, 460–464, 1974.

Kokhanovsky, A.: Optics of Light Scattering Media, Problems and Solutions, 2nd edn., Springer-Praxis, Chichester, UK, 2001.

Kong, J. A.: Electromagnetic Wave Theory, John Wiley, New York, 1986.

Kontu, A. and Pulliainen, J.: Simulation of spaceborne microwave radiometer measurements of snow cover using in situ data and brightness temperature modeling, IEEE T. Geosci. Remote, 48, 1031–1044, doi:10.1109/TGRS.2009.2030499, 2010.

Kontu, A., Lemmetyinen, J., Pulliainen, J., Seppänen, J., and Hallikainen, M.: Observation and modeling of the microwave brightness temperature of snow-covered frozen lakes and wetlands, IEEE T. Geosci. Remote, 52, 3275–3288, 2014.

Langlois, A., Royer, A., Derksen, C., Montpetit, B., Dupont, F., and Goïta, K.: Coupling the snow thermodynamic model SNOWPACK with the microwave emission model of layered snowpacks for subarctic and arctic snow water equivalent retrievals, Water Resour. Res., 48, W12524, doi:10.1029/2012WR012133, 2012.

Lemmetyinen, J., Pulliainen, J., Rees, A., Kontu, A., and Derksen, C.: Multiple-layer adaptation of HUT snow emission model: comparison with experimental data, IEEE T. Geosci. Remote, 48, 2781–2794, doi:10.1109/TGRS.2010.2041357, 2010.

Lemmetyinen, J., Kontu, A., Leppänen, L., Pulliainen, J., Wiesmann, A., Werner, C., Proksch, M., and Schneebeli, M.: Technical assistance for the development of an X- to Ku-Band Scatterometer during the NoSREx III experiment, Final report, ESA ESTEC Contract No. 22671/09/NL/JA, European Space Agency ESA ESTEC, Noordwijk, the Netherlands, 2013.

Lemmetyinen, J., Derksen, C., Toose, P., Proksch, M., Pulliainen, J., Kontu, A., Rautiainen, K., Seppänen, J., and Hallikainen, M.: Simulating seasonally and spatially varying snow cover brightness temperature using HUT snow emission model and retrieval of a microwave effective grain size, Remote Sens. Environ., 156, 71–95, 2015.

Löwe, H., Egli, L., Bartlett, S., Guala, M., and Manes, C.: On the evolution of the snow surface during snowfall, Geophys. Res. Lett., 34, L21507, doi:10.1029/2007GL031637, 2007.

Löwe, H., Spiegel, J. K., and Schneebeli, M.: Interfacial and structural relaxations of snow under isothermal conditions, J. Glaciol., 57, 499–510, doi:10.3189/002214311796905569, 2011.

Löwe, H., Riche, F., and Schneebeli, M.: A general treatment of snow microstructure exemplified by an improved relation for thermal conductivity, The Cryosphere, 7, 1473–1480, doi:10.5194/tc-7-1473-2013, 2013.

Manes, C., Guala, M., Löwe, H., Bartlett, S., Egli, L., and Lehning, M.: Statistical properties of fresh snow roughness, Water Resour. Res., 44, W11407, doi:10.1029/2007WR006689, 2008.

Matzl, M. and Schneebeli, M.: Measuring specific surface area of snow by near-infrared photography, J. Glaciol., 52, 558–564, doi:10.3189/172756506781828412, 2006.

Mätzler, C.: Applications of the interaction of microwaves with the seasonal snow cover, Remote Sens. Rev., 2, 259–387, 1987.

Mätzler, C.: Microwave Transmissivity of a Forest Canopy: Experiments Made with a Beech, Remote Sens. Environ., 48, 172–180, 1994.

Mätzler, C.: Microwave permittivity of dry snow, IEEE T. Geosci. Remote, 34, 573–581, doi:10.1109/36.485133, 1996.

Mätzler, C.: Improved Born approximation for scattering of radiation in a granular medium, J. Appl. Phys., 83, 6111, doi:10.1063/1.367496, 1998.

Mätzler, C.: HPACK, a bistatic radiative transfer model for microwave emission and backscattering of snowpacks, and validation by surface-based experiments, Tech. Rep. IAP research report 2000-4, University of Bern, Switzerland, 2000.

Mätzler, C.: Relation between grain-size and correlation length of snow, J. Glaciol., 48, 461–466, 2002.

Mätzler, C.: On the determination of surface emissivity from Satellite observations, IEEE Geosci. Remote S., 2, 160–163, doi:10.1109/LGRS.2004.842448, 2005.

Mätzler, C. and Melsheimer, C.: Radiative transfer and microwave radiometry, in: Thermal Microwave Radiation – Applications for Remote Sensing, ET Electromagnetic Waves Series 52, 1–23, Institution of Engineering and Technology (IET), London, UK, 2006.

Mätzler, C. and Rosenkranz, P.: Dependence of microwave brightness temperature on bistatic surface scattering: model functions and application to AMSU-A, IEEE T. Geosci. Remote, 45, 2130–2138, 2007.

Mätzler, C. and Wiesmann, A.: Extension of the microwave emission model of layered snowpacks to coarse-grained snow, Remote Sens. Environ., 70, 317–325, doi:10.1016/S0034-4257(99)00047-4, 1999.

Mätzler, C. and Wiesmann, A.: Documentation for MEMLS, Version 3, Microwave Emission Model of Layered Snowpacks, Tech. rep., Institute for Applied Physics, University of Bern, Switzerland, 2012.

Mironov, V., DeRoo, R., and Savin, I.: Temperature-dependable microwave dielectric model for an Arctic soil, IEEE T. Geosci. Remote, 48, 2544–2556, 2010.

Montpetit, B., Royer, A., Roy, A., Langlois, A., and Derksen, C.: Snow microwave emission modeling of ice lenses within a snowpack using the microwave emission model for layered snowpacks, IEEE T. Geosci. Remote, 51, 4705–4717, 2013.

Painter, T., Molotch, N., Cassidy, M., Flanner, M., and Steffen, K.: Instruments and methods: contact spectroscopy for determination of stratigraphy of snow optical grain size, J. Glaciol., 53, 121–127, doi:10.3189/172756507781833947, 2007.

Picard, G., Brucker, L., Roy, A., Dupont, F., Fily, M., Royer, A., and Harlow, C.: Simulation of the microwave emission of multi-layered snowpacks using the Dense Media Radiative transfer theory: the DMRT-ML model, Geosci. Model Dev., 6, 1061–1078, doi:10.5194/gmd-6-1061-2013, 2013.

Proksch, M. and Schneebeli, M.: Development of snow retrieval algorithms for CoReH$_2$O grain size estimator: procedures for objective snow pack structure parameters, Tech. Rep. 22830/09/NL/JC, European Space Agency, Noordwijk, the Netherlands, 2012.

Proksch, M., Löwe, H., and Schneebeli, M.: Density, specific surface area and correlation length of snow measured by high-resolution penetrometry, J. Geophys. Res., accepted, doi:10.1002/2014JF003266, 2015.

Pulliainen, J., Grandell, J., and Hallikainen, M.: HUT snow emission model and its applicability to snow water equivalent retrieval, IEEE T. Geosci. Remote, 37, 1378–1390, doi:10.1109/36.763302, 1999.

Rautiainen, K., Lemmetyinen, J., Pulliainen, J., Vehviläinen, Drusch, M., Kontu, A., Kainulainen, J., and Seppänen, J.: L-band radiometer observations of soil processes in boreal and subarctic environments, IEEE T. Geosci. Remote, 50, 1483–1497, 2012.

Rees, A., Lemmetyinen, J., Derksen, C., Pulliainen, J., and English, M.: Observed and modelled effects of ice lens formation on passive microwave brightness temperatures over snow covered tundra, Remote Sens. Environ., 114, 116–126, doi:10.1016/j.rse.2009.08.013, 2010.

Rott, H., Yueh, S., Cline, D., and Duguay, C.: Cold regions hydrology high-resolution observatory for snow and cold land processes, P. IEEE, 98, 752–765, doi:10.1109/JPROC.2009.2038947, 2010.

Roy, A., Picard, G., Royer, A., Montpetit, B., Dupont, F., and Langlois, A.: Brightness temperature simulations of the Canadian seasonal snowpack driven by measurements of snow specific surface area, IEEE T. Geosci. Remote, 51, 4692–4704, 2013.

Schneebeli, M. and Johnson, J.: A constant-speed penetrometer for high-resolution snow stratigraphy, Ann. Glaciol., 26, 107–111, 1998.

Schneebeli, M. and Sokratov, S.: Tomography of temperature gradient metamorphism of snow and associated changes in heat conductivity, Hydrol. Processes, 18, 3655–3665, doi:10.1002/hyp.5800, 2004.

Schwank, M., Rautiainen, K., Mätzler, C., Stähli, M., Lemmetyinen, J., Pulliainen, J., Vehviläinen, J., Kontu, A., Ikonen, J., Ménard, C. B., Drusch, M., Wiesmann, A., and Wegmüller, U.: Model for microwave emission of a snow-covered ground with focus on L band, Remote Sens. Environ., 154, 180–191, doi:10.1016/j.rse.2014.08.029, 2014.

Takala, M., Luojus, K., Pulliainen, J., Derksen, C., Lemmetyinen, J., Kämä, Koskinen, J., and Bojkov, B.: Estimating northern hemisphere snow water equivalent for climate research through assimilation of space-borne radiometer data and ground-based measurements, Remote Sens. Environ., 115, 3517–3529, doi:10.1016/j.rse.2011.08.014, 2011.

Tan, S., Chang, W., Tsang, L., Lemmetyinen, J., and Proksch, M.: Modeling both active and passive microwave remote sensing of snow using dense media radiative transfer (DMRT) theory with multiple scattering and backscattering enhancement, IEEE J. Sel. Top. Appl., in review, 2015.

Tedesco, M. and Kim, E.: Intercomparison of electromagnetic models for passive microwave remote sensing of snow, IEEE T. Geosci. Remote, 44, 2654–2666, 2006.

Toure, A. M., Goïta, K., Royer, A., Kim, E. J., Durand, M., Margulis, S. A., and Lu, H.: A case study of using a multilayered thermodynamical snow model for radiance assimilation, IEEE T. Geosci. Remote, 48, 2828–2837, 2011.

Tsang, L., Blanchard, A., Newton, R., and Kong, J. A.: A simple relation between active and passive microwave remote sensing measurements of earth terrain, IEEE T. Geosci. Remote, 20, 482–485, 1982.

Tsang, L., Pan, J., Liang, D., Li, Z., Cline, D., and Tan, Y.: Modeling active microwave remote sensing of snow using dense media radiative transfer (DMRT) theory with multiple-scattering effects, IEEE T. Geosci. Remote, 45, 990–1004, 2007.

Ulaby, F., Moore, R., and Fung, A.: Microwave Remote Sensing Active and Passive, Vol. I, Microwave Remote Sensing Fundamentals and Radiometry, Addison-Wesley Publishing Company, Reading, Mass., USA, 1981.

Ulaby, F., Moore, R., and Fung, A.: Microwave Remote Sensing Active and Passive, Vol. II, Radar Remote Sensing and Surface Scattering and Emission Theory, Addison-Wesley Publishing Company, Reading, Mass., USA, 1982.

Ulaby, F., Stiles, W., and Abdelrazik, M.: Snow cover influence on backscattering from terrain, IEEE T. Geosci. Remote, 22, 126–133, 1984.

Von Lerber, A., Sarvas, J., and Pulliainen, J.: Modeling snow volume backscatter combining the radiative transfer theory and the discrete dipole approximation, in: IEEE International Conference on Geoscience and Remote Sensing, Symposium, 31 July 2006–4 August 2006, Denver, CO, USA, 481–484, doi:10.1109/IGARSS.2006.128, 2006.

Wegmüller, U. and Mätzler, C.: Rough bare soil reflectivity model, IEEE T. Geosci. Remote, 37, 1391–1395, 1999.

Weise, T.: Radiometric and Structural Measurements of Snow, Ph.D. thesis, Institute of Applied Physics, University of Bern, Switzerland, 1996.

Werner, C., Wiesmann, A., Strozzi, T., Schneebeli, M., and Mätzler, C.: The snowscat ground-based polarimetric scatterometer: calibration and initial measurements from Davos Switzerland, in: IEEE

International Geoscience and Remote Sensing Symposium (IGARSS), 25–30 July 2010, Honolulu, HI, USA, 2363–2366, 2010.

Wiesmann, A.: Catalog of Radiometric and Structural snow sample measurements, Tech. Rep. IAP research report 97-1, University of Bern, Switzerland, 1997.

Wiesmann, A. and Mätzler, C.: Microwave emission model of layered snowpacks, Remote Sens. Environ., 70, 307–316, doi:10.1016/S0034-4257(99)00046-2, 1999.

Wiesmann, A., Mätzler, C., and Weise, T.: Radiometric and structural measurements of snow samples, Radio Sci., 33, 273–289, 1998.

Xu, X.: Electromagnetic models of co/cross polarization of bicontinuous/DMRT in radar remote sensing of terrestrial snow at X- and Ku-band for CoReH$_2$O and SCLP applications, IEEE J. Sel. Top. Appl., 5, 1024–1032, 2012.

Table 1. Primary input parameters used in MEMLS3&a, with snow input parameters for each snow layer (upper part) and general model parameters (lower part). In addition the value and unit of the parameter, as well as a typical way of determination are indicated.

Parameter	Value and Unit	Determination
density ρ	[0–917] kg m^{-3}	traditional[1], SMP, CT
exponential correlation length l_{ex}	mm	SMP, CT, (NIP)[2]
volume fraction of liquid water	[0–1]	traditional[1], dielectric[3]
snow salinity	[0–0.1] ppt	electric conductivity
layer thickness	cm	traditional[1], SMP, NIP, CT
temperature T	K	traditional[1]
physical ground temperature T_0	K	thermometer
snow-ground reflectivity s_0	[0–1]	modeled[4]
specular snow-ground reflectivity $s_{\mathrm{s}0}$	[0–1]	estimated from s_0[5]
cross polarization ratio q	[0–1]	empirical
mean slope of surface undulations m	[0–∞]	empirical

[1] Fierz et al. (2009).

[2] In combination with a density measurement (Eqs. 16 and 17).

[3] Denoth et al. (1984).

[4] Wegmüller and Mätzler (1999).

[5] See text, Sect. 4.1.2.
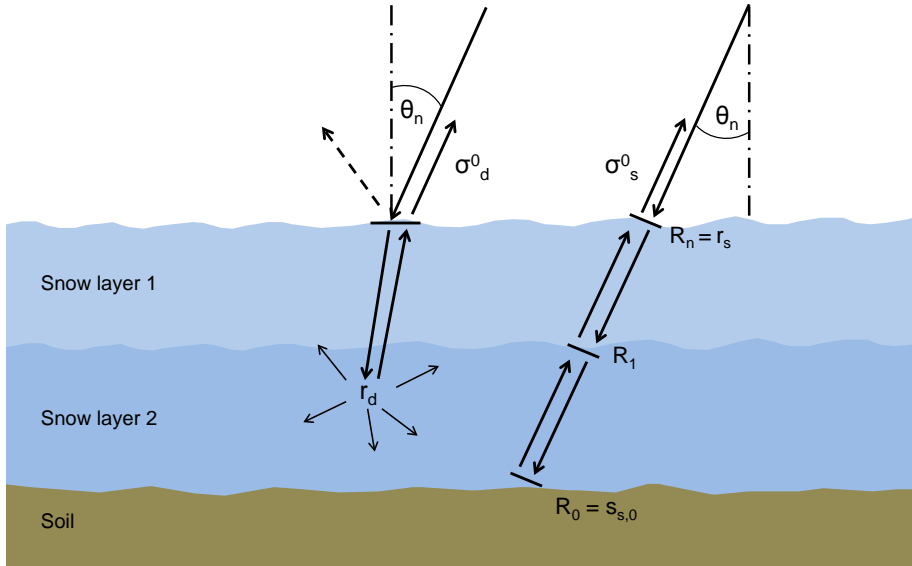
Figure 1. Snowpack (blue) with slightly undulated snow surface and layers. Waves incident at nadir angle θ_n are refracted at the snow surface followed by volume scattering with backscatter ~~; specular reflection without backscatter~~ σ_d^0 (left)~~.~~; Specular backscatter σ_s^0 from a slightly tilted patch of the surface~~(right)~~, soil and layer interfaces (~~not shown~~right). Diffuse r_d and specular reflectivities $r_s = R_n$, R_0 and R_1 are indicated.
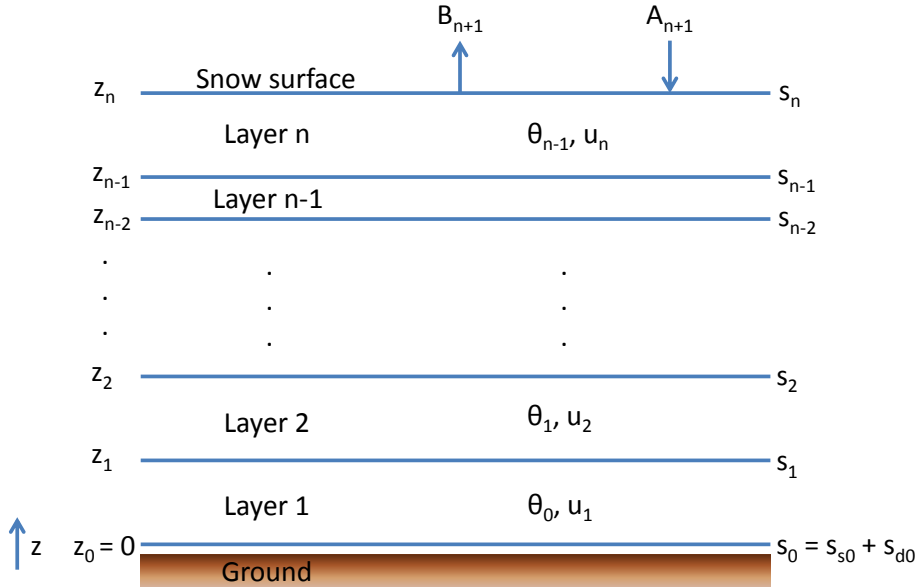
Figure 2. Geometry of the n-layered snowpack with up- and downwelling intensities A and B. Height z_j, transmissivity u_j of directed radiation, refracted angle θ_{j-1} and interface reflectivity s_j for layer number j ranging from 1 (bottom) to n (top). Snow-ground reflectivity s_0, consisting of specular s_{s0} and diffuse component s_{d0}.
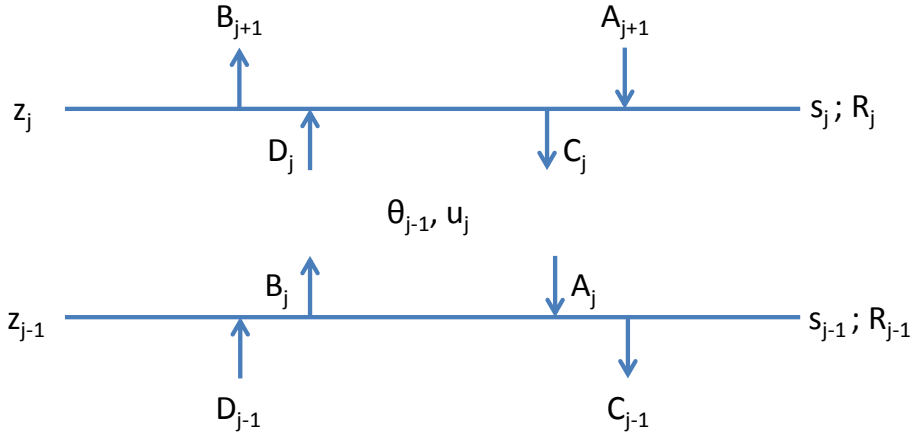
Figure 3. The parameters of a selected layer j: height z_j, up- and downwelling intensities A, B, C, D, transmissivity u_j of directed radiation, refracted angle θ_{j-1}, interface reflectivity s_j and specular reflectivity R_j.
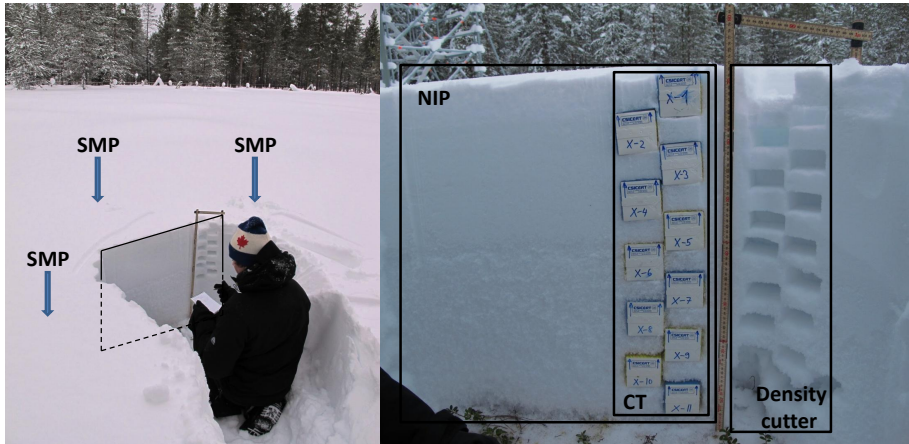
Figure 4. Left: snowpit overview with the locations of the SnowMicroPen (SMP) measurements (arrows) surrounding the profile wall (black rectangular). Right: close-up of the profile wall, with locations of Near Infra-red Photography (NIP), Computed Tomography (CT) and density cutter measurements.
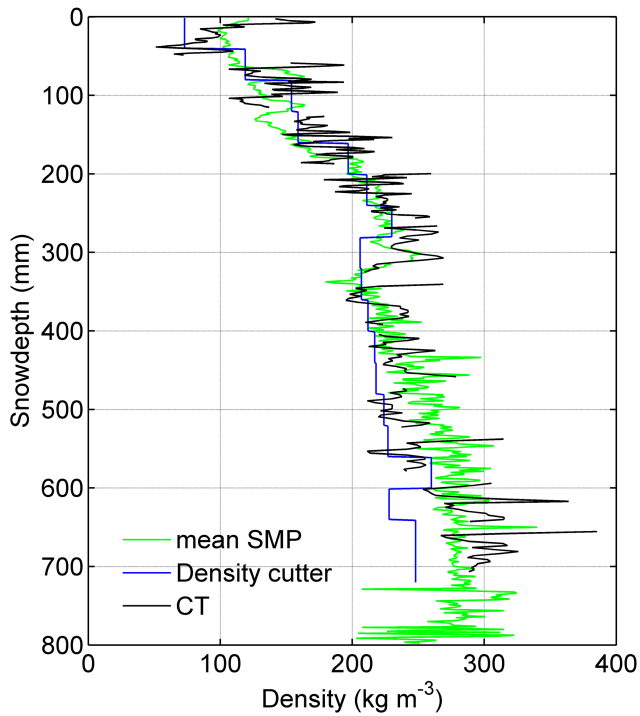
Figure 5. Density profile derived by SMP (green), μCT (black) and density cutter (blue). The green line is the average of three neighboring SMP measurements.
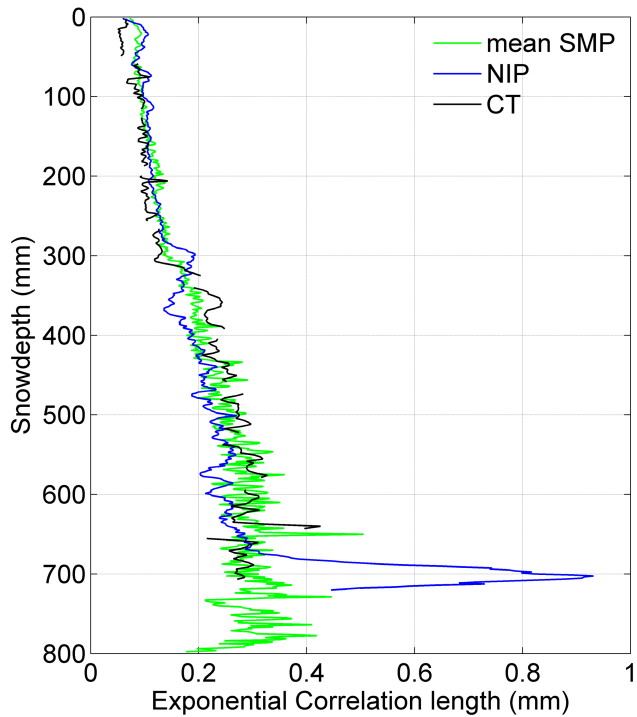
Figure 6. Correlation length profile derived by SMP (green), μCT (black) and NIP (blue). The blue line is the correlation length derived from the SSA measured by NIP according to Mätzler (2002).
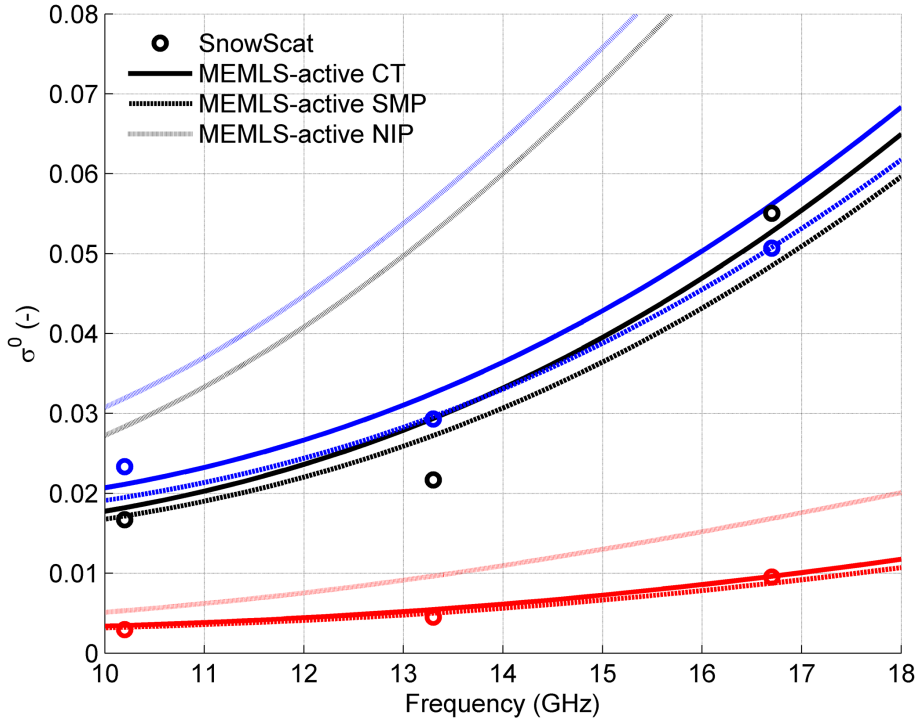
Figure 7. σ^0 measured by SnowScat (circles) and modeled by MEMLS3&a (lines) with SMP (solid), CT (dashed) and NIP (dotted) input. MEMLS3&a runs are performed with the snow-ground reflectivity s_0 calculated by Wegmüller and Mätzler (1999), and $s_{s0,h} = 0.75 \ s_{0,h}$, $s_{s0,v} = 0.75 \ s_{0,v}$. The mean slope of surface undulation was set to $m = 0.1$ and the cross polarization ratio $q = 0.15$. Colors represent polarization, with vv – black, hh – blue and hv – red.
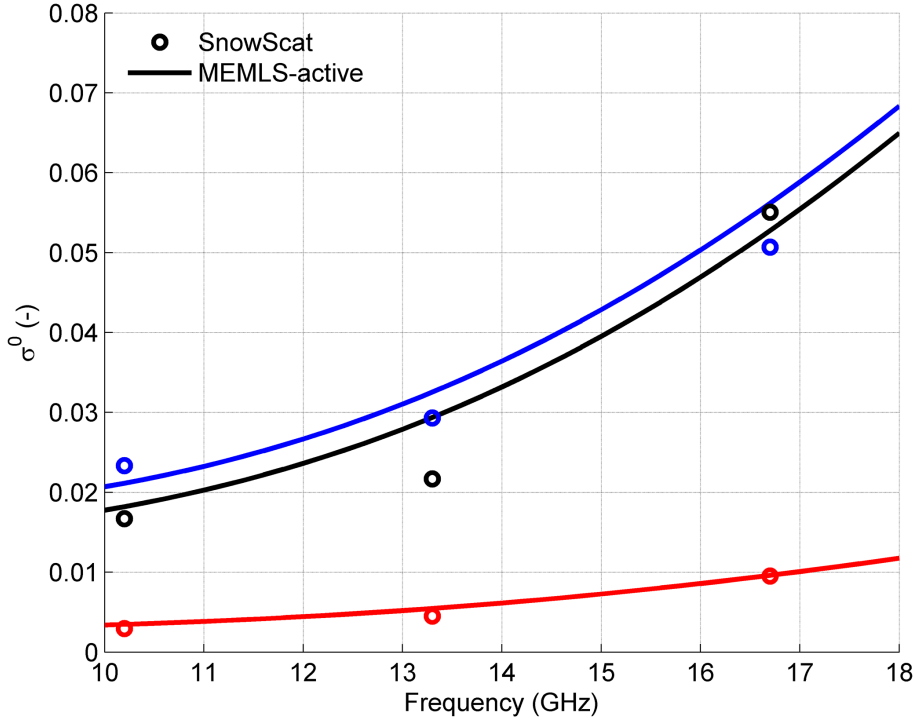
Figure 8. σ^0 at incidence angle $50°$ measured by SnowScat (circles) and modeled by MEMLS3&a with CT input (lines) for best fit parameters $s_{s0,h} = 0.75 \cdot s_{0,h}$, $s_{s0,v} = 0.75 \cdot s_{0,v}$, $q = 0.15$ and $m = 0.1$. Colors represent polarization, with vv – black, hh – blue and hv – red.
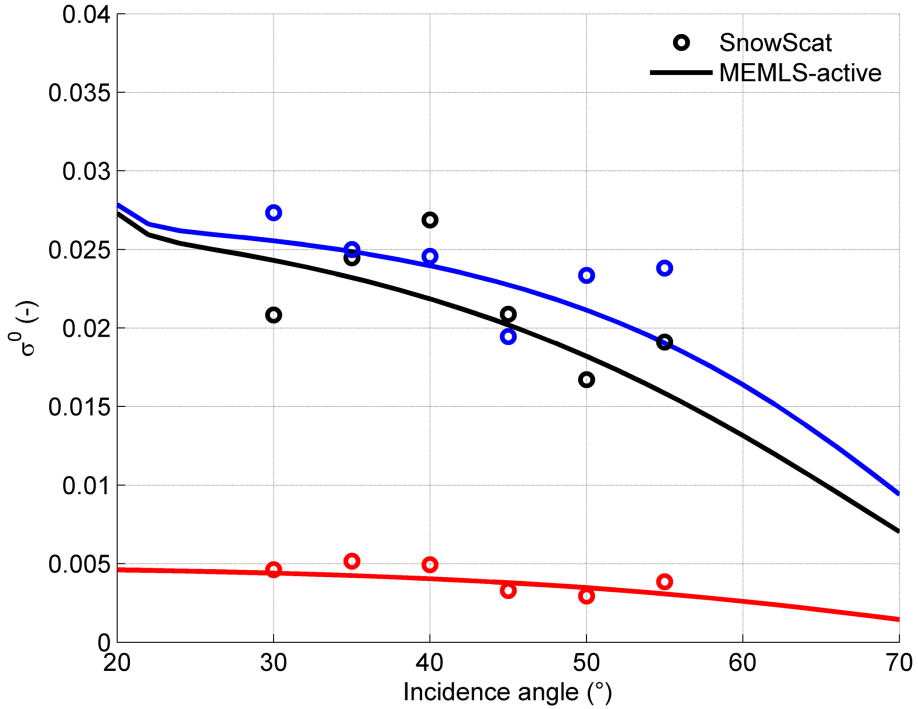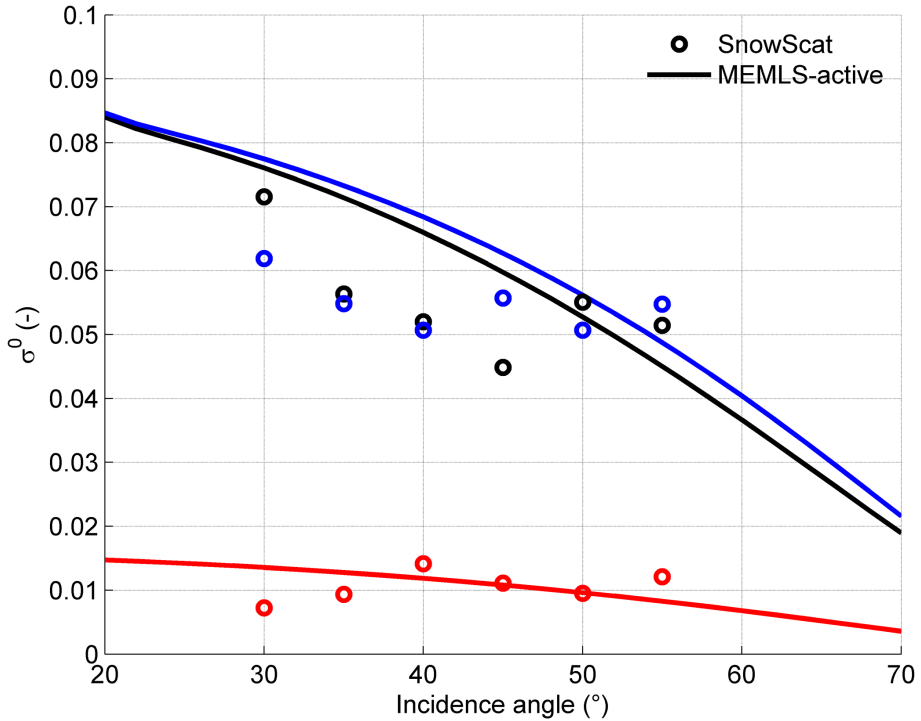
Figure 9. σ^0 at 10.2 GHz measured by SnowScat (circles) and modeled by MEMLS3&a with CT input (lines). Colors represent polarization, with vv – black, hh – blue and hv – red. Best fit parameters according to Fig. 8.
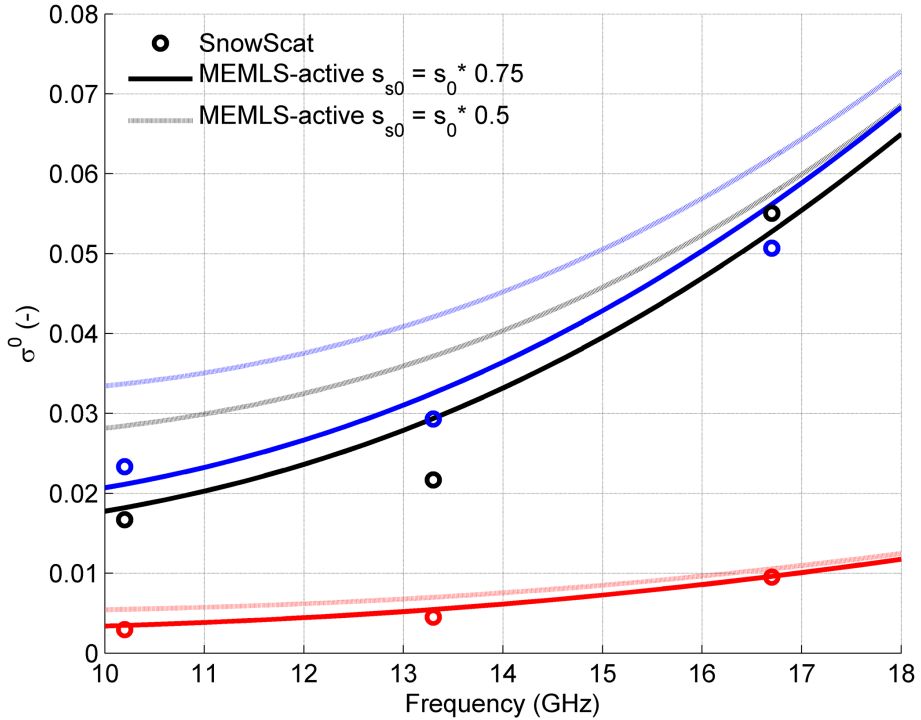
Figure 10. σ^0 at 16.7 GHz measured by SnowScat (circles) and modeled by MEMLS3&a with CT input (lines). Colors represent polarization, with vv – black, hh – blue and hv – red. Best fit parameters according to Fig. 8.

Figure 11. σ^0 at incidence angle $50°$ measured by SnowScat (circles) and modeled by MEMLS3&a with CT input (lines) for different specular snow-ground reflectivities s_{s0}. Higher s_{s0} values lead to lower σ^0 values and vice versa. Colors represent polarization, with vv – black, hh – blue and hv – red. Best fit parameters according to Fig. 8.
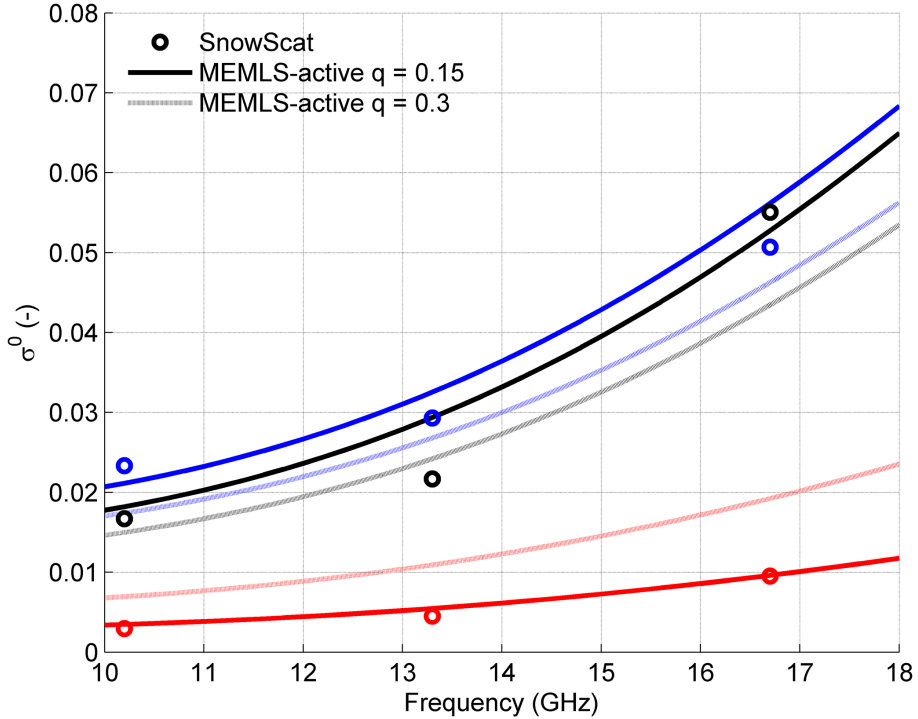
Figure 12. σ^0 at incidence angle $50°$ measured by SnowScat (circles) and modeled by MEMLS3&a with CT input (lines) for different cross polarization ratios q. Higher q ratios lead to lower σ^0 values for co-polarization and higher σ^0 values for cross-polarization. Colors represent polarization, with vv – black, hh – blue and hv – red. Best fit parameters according to Fig. 8.
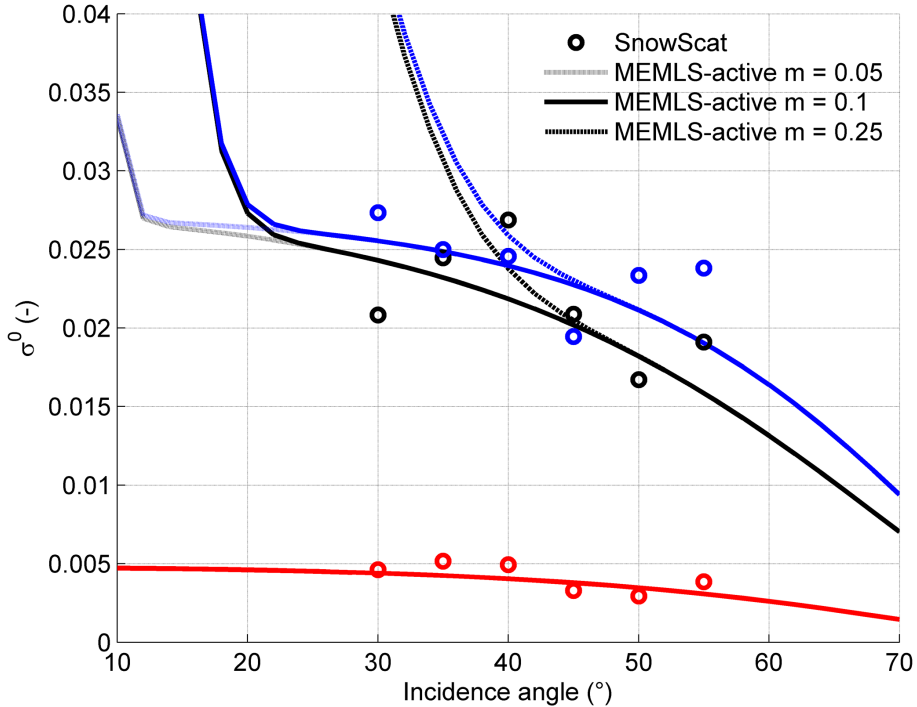
Figure 13. σ^0 measured by SnowScat (circles) and modeled by MEMLS3&a with CT input (lines) at 10.65 GHz for different mean slope of surface undulations m. ~~The effect of m is limited to small incidence angles.~~ Colors represent polarization, with vv – black, hh – blue and hv – red. Best fit parameters according to Fig. 8.
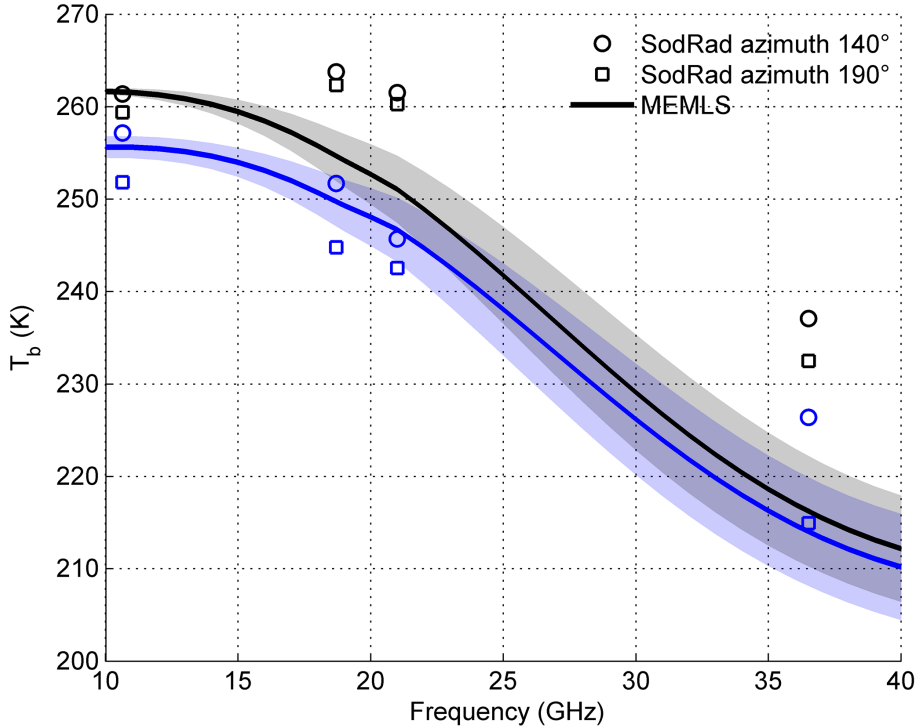
Figure 14. T_b measured by SodRad at an azimuth angle of 190° (circles) and at 140° (squares). T_b modeled by MEMLS from 15 SMP measurements, average (lines) with standard deviation (shaded). Colors represent polarization, with v – black and h – blue.

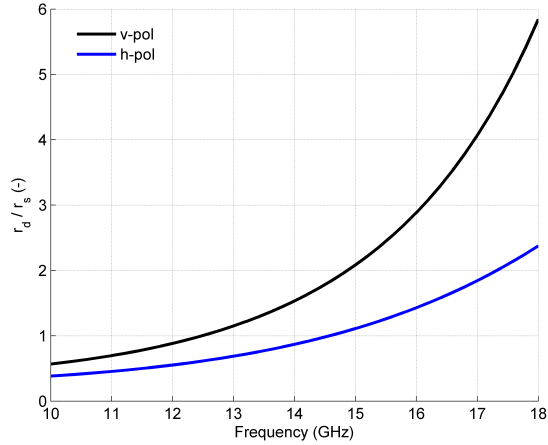**Figure 15.** View of about $1\,\mathrm{m}^2$ of the snow-free surface at the radiometer test site in Sodankylä, Finland.

Figure 16. Ratio of the simulated diffuse (r_d) and specular (r_s) reflectivity at $50°$ incidence angle per frequency, for the best fit parameters according to Fig. 8.